3rd of 3 files

Chapters 8 and 9, Appendices and References

STUDIES OF THE MAGNETIC PROPERTIES AND MICROSTRUCTURES OF TWO RARE EARTH-TRANSITION METAL TYPE MAGNETIC ALLOYS

By
Tony Bailey

A thesis submitted for the degree of
Doctor of Philosophy

Department of Metallurgy and Materials,
Faculty of Science and Engineering,
University of Birmingham.
August 1985

CHAPTER EIGHT

RESULTS AND DISCUSSION ON THE Nd-Fe-B ALLOY

8.1 Introduction

This chapter contains the results of the investigations on the Nd-Fe-B alloy. The microscope studies, X-ray microanalysis and microhardness measurements of the bulk specimens are discussed first. This is followed by a discussion of similar investigations on the sintered samples.

8.2 Studies of the Bulk Alloy

8.2.1 Optical Metallography of the Bulk Samples

8.2.1i The "As Cast" Sample

The optical micrograph of the "as cast" specimen is shown in fig. 8.1. Three phases can be observed:

1. A matrix phase (A).
2. An intergranular phase (B).
3. A globular phase (C).

Previous investigations have shown the matrix phase to have a tetragonal structure with the composition $Nd_2Fe_{14}B$ (refs. 89, 117) and this phase is mainly responsible for the magnetic properties of the sintered permanent magnets (see for example, ref. 118). The intergranular phase B is a low melting point phase, which is Nd-rich (refs. 88, 117). The globular phase C is present only in the "as cast" specimen and has been shown to be

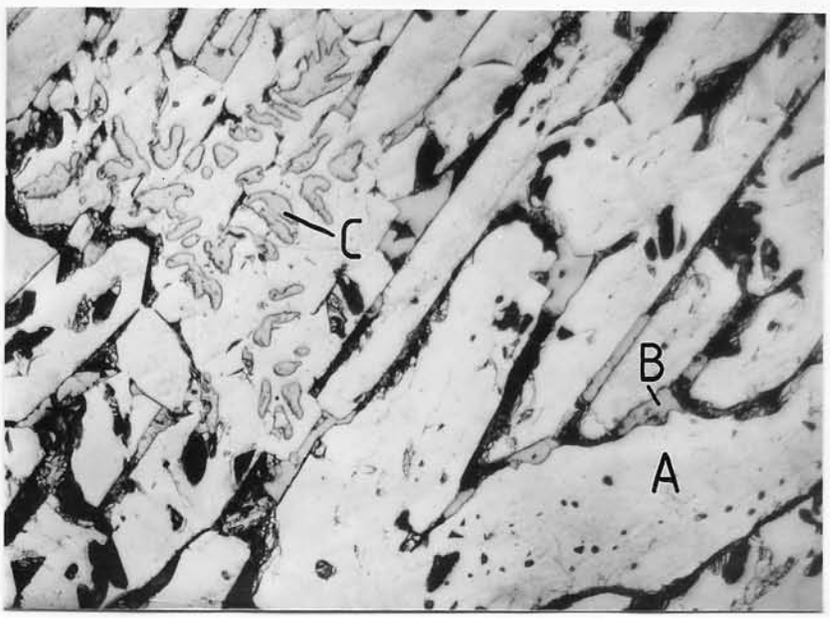

Fig. 8.1 Optical micrograph of "as cast" Nd-Fe-B. (x 400).

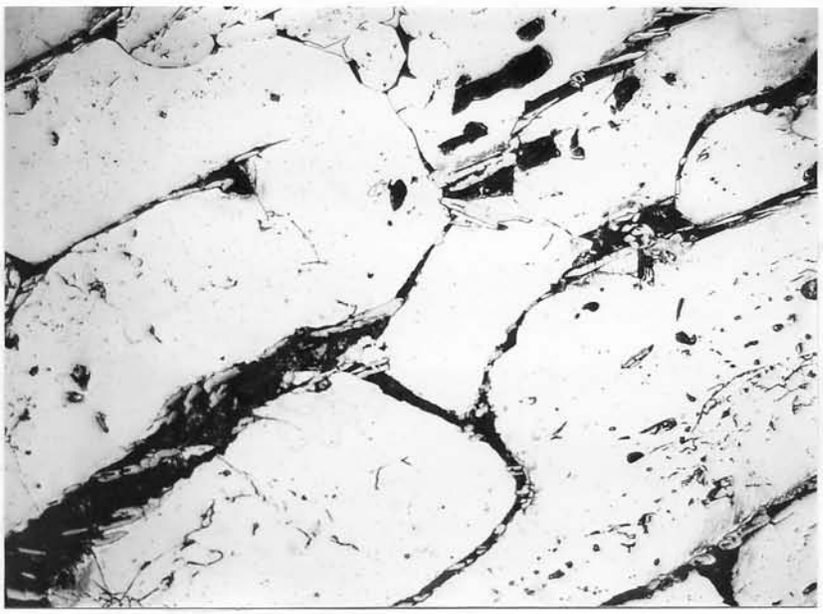

Fig. 8.2 Optical micrograph of bulk sample SST at 1100°C and quenched. (x 400).

free Fe (refs. 88, 117), which is a result of non-equilibrium cooling, during production of the bulk alloy.

The black regions are areas where the intergranular phase has been "pulled out" on polishing due to its relative softness.

8.2.1ii The Sample S.S.T. at 1100°C and Quenched

The optical micrograph for the sample quenched from a S.S.T. temperature of 1100°C is shown in fig. 8.2. There is some difference in the microstructure compared with the "as cast" sample. There appears to have been some grain growth in this specimen, indicated by the larger spacing of the intergranular phase and the free-Fe is now absent. Work has shown that free-Fe is only formed in this alloy when the cooling rate is low (ref. 119), as higher cooling rates tend to promote the formation of primary $Nd_2Fe_{14}B$ rather than primary Fe from the melt. Thus, at the S.S.T. temperature of 1100°C, all the free-Fe present in the "as-cast" specimen has dissolved and not reappeared on cooling due to the high cooling rate.

8.2.1iii The Sample S.S.T. at 1100°C and Furnace Cooled

The difference in the microstructure of this specimen (see fig. 8.3) is due to the fact that the sample was sectioned perpendicular to the columnar grains observed in figs. 8.1 and 8.2.

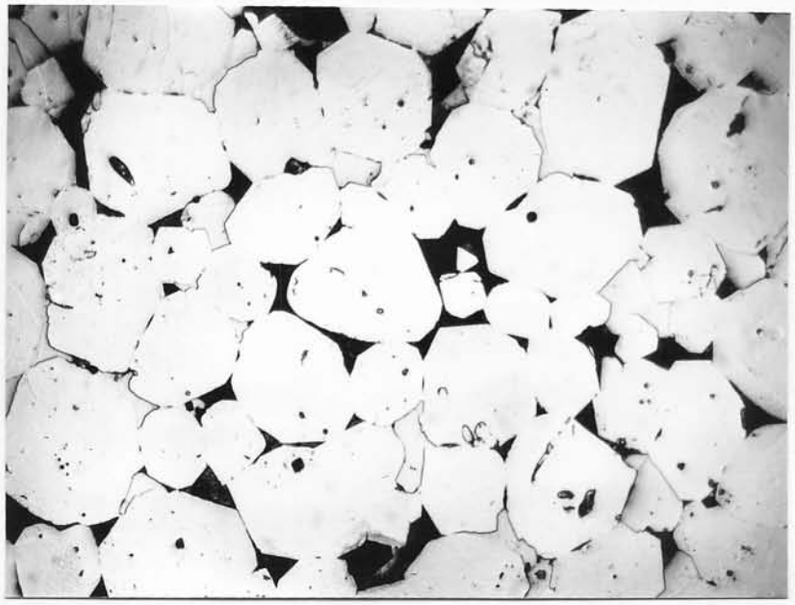

Fig. 8.3 Optical micrograph of bulk sample SST at 1100°C and furnace cooled. (x 400).

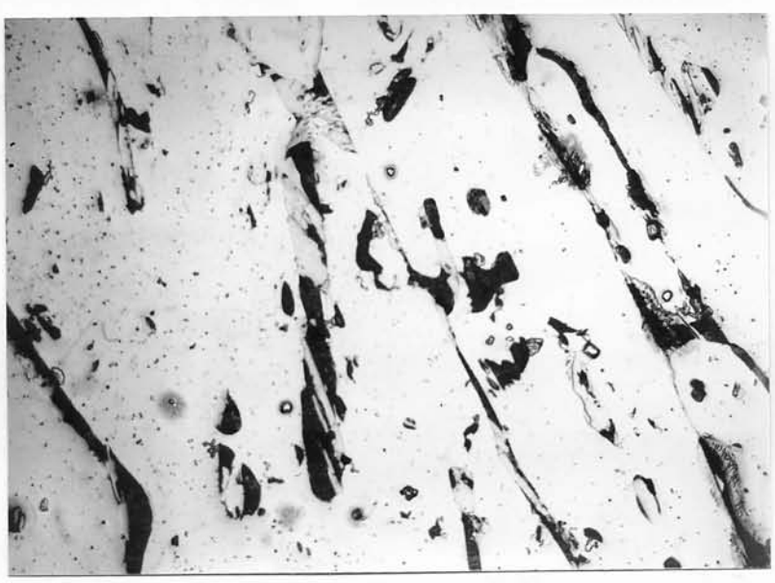

Fig. 8.4 Optical micrograph of bulk sample SST at 1100°C, quenched and aged at 600°C for 100 hours. (x 250).

Two phases can be observed: a matrix phase and an intergranular phase.

8.2.1iv The Sample S.S.T. at 1100°C, Quenched and then Aged at 600°C for about 100 hours

The microstructure of this specimen (see Fig. 8.4) indicates some grain growth on ageing at 600°C. There are also some dark spots within the grains which might be (1) a polishing effect, (2) a phase associated with the ageing treatment, or (3) micropores associated with the casting of the alloy.

8.2.1v The Sample S.S.T. at 1100°C, Furnace Cooled and then Aged at 600°C for about 100 hours

The specimen aged at 600°C for an extended period after furnace cooling from 1100°C, shows a large amount of grain growth (see fig. 8.5). A matrix phase and an intergranular phase can be seen, the grain growth being indicated by the separation between the intergranular phase. Lee (ref. 120) has noted grain growth in permanent magnet specimens produced via melt-spun ribbons. It is possible that the furnace cooling treatment involves some additional grain growth.

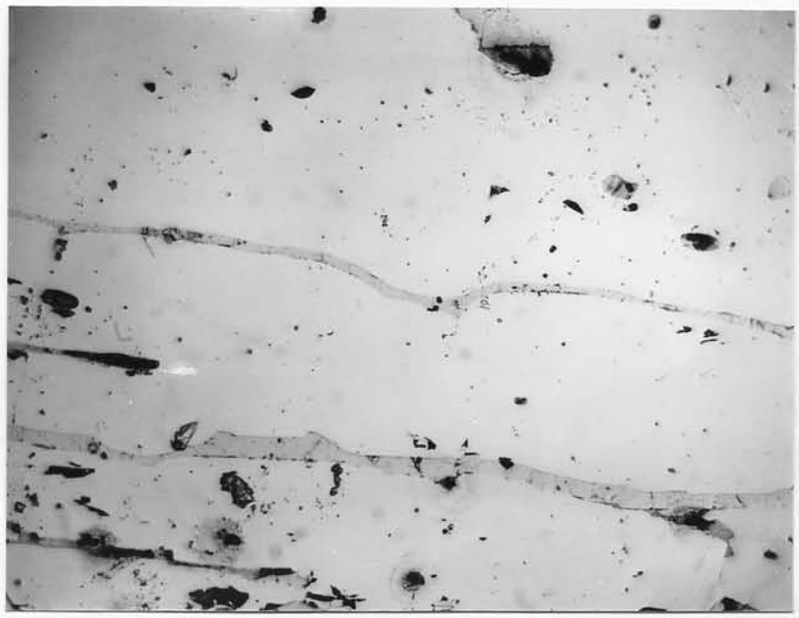

Fig. 8.5 Optical micrograph of bulk specimen SST at 1100°C, furnace cooled and aged at 600°C for 100 hours. (x 250).

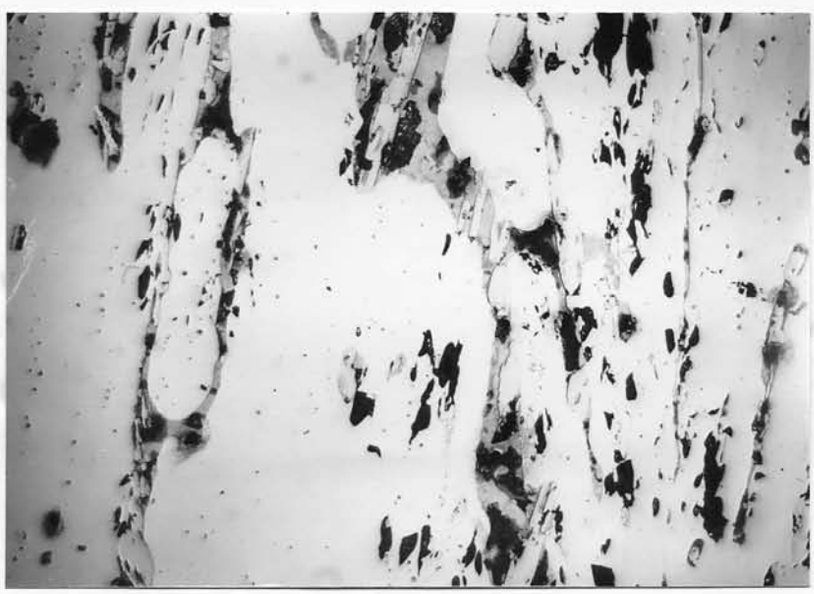

Fig. 8.6 Optical micrograph of bulk specimen SST at 1100°C, quenched and aged at 660°C for 100 hours. (x 250).

8.2.1vi The Sample S.S.T. at 1100°C, Quenched and then Aged at 660°C for about 100 hours

The optical micrograph is shown in fig. 8.6. Two phases can be seen: the matrix phase and an intergranular phase. The intergranular phase consists of light grey and dark grey regions. These may be two different phases which have similar melting points; alternatively they may represent a polishing effect. Two intergranular phases have been observed previously consisting of free Nd and a Nd-B binary phase (ref. 117). Therefore, the ageing temperature of 660°C may be concurrent with the appearance of a second intergranular phase.

8.2.2 SEM Studies of the Bulk Alloy

Secondary electron and backscattered electron studies were made on the SEM to determine whether any phases were present in the bulk alloys that could not be observed on the optical microscope.

8.2.2i The "As Cast" Sample

The backscattered electron micrograph is shown in fig. 8.7 and three phases can be seen:

1. A grey matrix phase (A).
2. A light grey intergranular phase (B).
3. A dark grey globular phase (C).

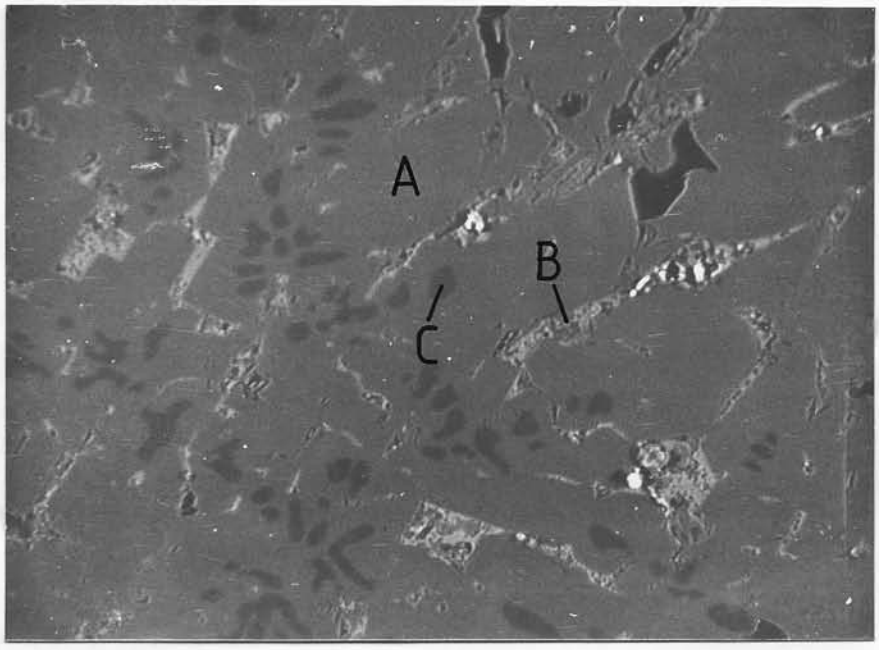

Fig. 8.7 Backscattered SEM micrograph of "as cast" sample. (x 320).

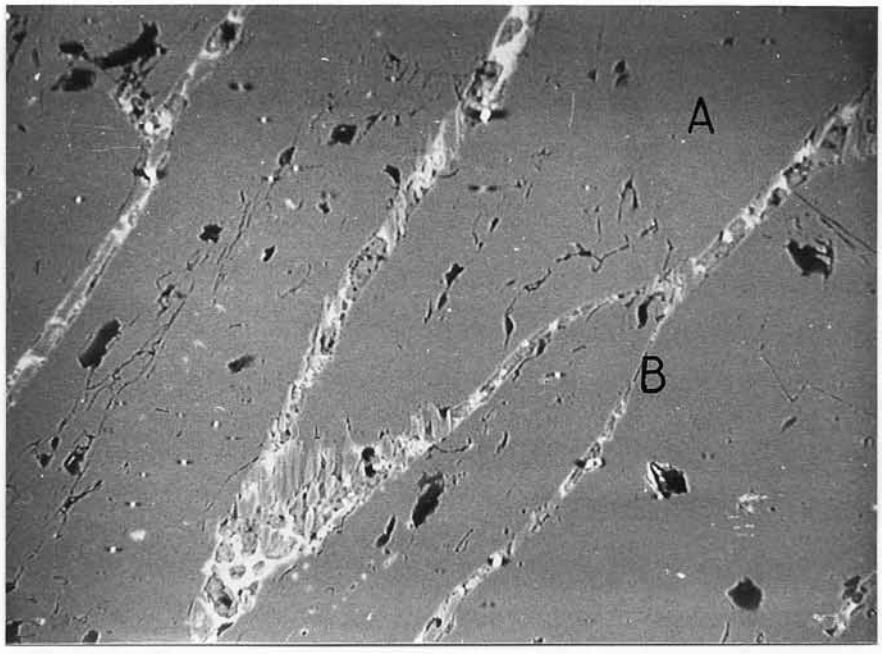

Fig. 8.8a Backscattered SEM micrograph of bulk sample SST at 1100°C and quenched. (x 320).

As was discussed in section 8.2.1i, the phases A, B and C correspond to a tetragonal $Nd_2Fe_{14}B$ phase, a Nd-rich phase and free Fe respectively. These phases have been observed in melt-spun ribbons by Hadjipanayis (ref. 121) using transmission electron microscopy (TEM).

8.2.2ii The Sample S.S.T. at 1100°C and Quenched

The backscattered electron micrograph is shown in fig. 8.8a and the intergranular phase and matrix phase are present.

8.2.2iii The Sample S.S.T. at 1100°C and Furnace Cooled

The backscattered electron micrograph is shown in fig. 8.8b and the intergranular phase (light phase) and matrix are present.

8.2.2iv The Sample S.S.T. at 1100°C, Quenched and then Aged at 600°C for 100 hours

The secondary electron micrograph of this specimen is shown in figure 8.9. Within the columnar grains light and dark regions can be seen; these represent the presence of magnetic domains. The shape of the domain patterns indicate that the c-axis of the tetragonal matrix phase lies in the plane of the micrograph. This type of domain contrast was exhibited only in this specimen and could be a result of material decorating the domain walls or possibly that the contrast has to be very finely altered in the SEM to achieve such an image.

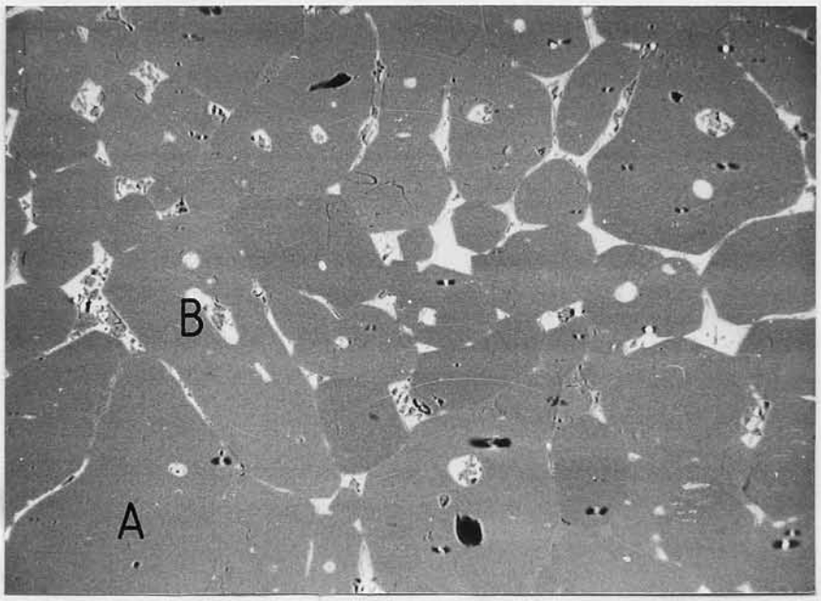

Fig. 8.8b Backscattered SEM micrograph of bulk sample SST at 1100°C and furnace cooled. (x 320).

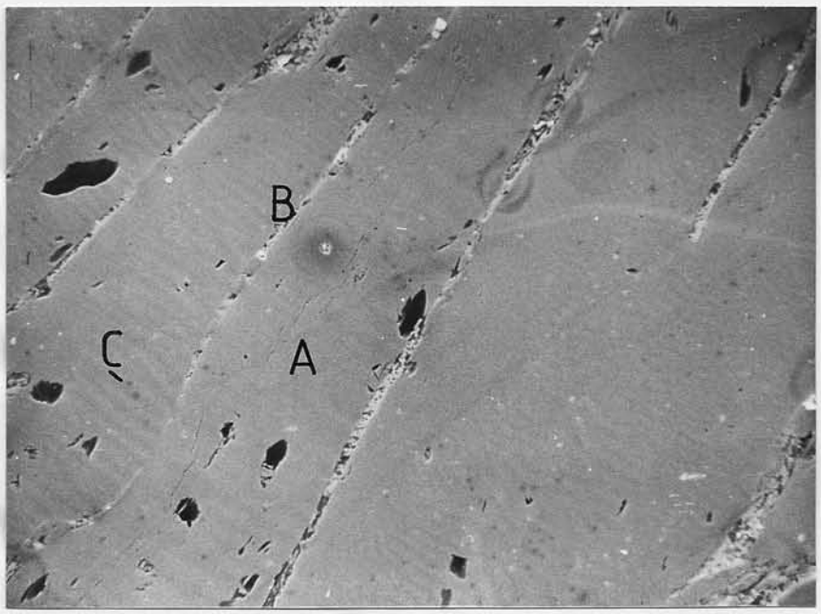

Fig. 8.9 Secondary SEM micrograph of bulk sample SST at 1100°C, quenched and aged at 600°C for 100 hours. (x 320).

Three phases were observed in this specimen:

1. A grey matrix phase (A).
2. A light grey intergranular phase (B).
3. A small dark phase within the columnar grain (C).

The presence of the phase (C) is a result of the ageing treatment after quenching and the EDAX analyses (see later) show that this phase has a different composition than that of the matrix.

These three phases were also observed in the sample that had been furnace cooled and then aged at 600°C, but to a lesser extent. Thus the presence of the phase within the columnar grains may be the result of the quenching treatment. The phase within the grains was not observed at all in the specimen aged at 660°C after quenching from 1100°C. This may be a result of the specimen being aged at too high an ageing temperature for this phase to exist.

8.2.3 X-ray Microanalysis Studies of the Bulk Samples

The EDAX studies were limited due to the fact that with the present detector boron could not be detected. Therefore, in all the X-ray microanalysis studies the boron substitution composition is given as x, an unknown. More detailed studies to determine the boron content in the samples must involve the use of a windowless detector, or wet chemical analysis.

The results of the measurements on the bulk samples are given in table 8.1. The matrix phase has the composition $Nd_2Fe_{14}B_x$, which agrees

Table 8.1

EDAX measurements on the bulk Nd-Fe-B Specimens

Heat Treatment	Area Details	Substitution Composition (±0.3-0.5)
As cast As cast (see fig. 8.7)	Matrix phase (A) Intergranular phase (B)	$Nd_2Fe_{14}B_x$ $Nd_{15}FeB_x$
S.S.T. at 1100°C, quenched S.S.T. at 1100°C, quenched (see fig. 8.8a)	Matrix phase (A) Intergranular phase (B)	$Nd_2Fe_{14}B_x$ $Nd_{19}FeB_x$
S.S.T. at 1100°C, furnace cooled (see fig. 8.8b)	Matrix phase (A) Intergranular phase (B)	$Nd_2Fe_{14}B_x$ $Nd_{18}FeB_x$
S.S.T. at 1100°C, quenched and aged at 600°C for 100 hours (see fig. 8.9)	Matrix phase (A) Intergranular phase (B) Phase within matrix (C)	$Nd_2Fe_{13}B_x$ $Nd_{24}FeB_x$ $Nd_{12}Fe_5B_x$
S.S.T. at 1100°C, furnace cooled and aged at 600°C for 100 hours	Matrix phase Intergranular phase Phase within matrix	$Nd_2Fe_{13}B_x$ $Nd_{24}FeB_x$ $Nd_{12}FeB_x$
S.S.T. at 1100°C, quenched and aged at 660°C for 100 hours.	Matrix phase Intergranular phase	$Nd_2Fe_{13}B_x$ $Nd_{20}FeB_x$

with other data (refs. 89, 117). On isothermal ageing at 600°C and 660°C for 100 hours, the composition of the matrix appears to be lower in Fe and has the composition $Nd_2Fe_{13}B_x$; allowing for the errors quoted in table 8.1 however, would give a matrix composition similar to that in the bulk material.

On ageing at 600°C for 100 hours, the quenched and furnace cooled samples have an intergranular phase of composition $Nd_{24}FeB_x$, which is richer in Nd than the "as cast", "as-quenched" and "as-furnace cooled" samples. In addition, on ageing at 600°C the quenched and furnace cooled samples have intra-columnar phases (see (C) in fig. 8.9) of composition $Nd_{12}Fe_5B_x$ and $Nd_{12}FeB_x$ respectively. These intracolumnar phases disappear on ageing at 660°C. Studies on sintered samples have shown the presence of a boron rich phase (see for example refs. 91, 118) but not of a phase composition as high in Nd as found in phase (C); the boron rich phase was not found in the bulk samples using SEM studies.

The amount of Nd in the "as cast" intergranular phase is lower than in all the heat treated specimens. The specimens aged at 600°C have the highest concentration of Nd in the intergranular phase (composition: $Nd_{24}FeB_x$).

8.2.4 Microhardness Studies on the Bulk Samples

The results of the microhardness studies on the bulk samples quenched or furnace cooled from 1100°C and then aged at 600°C for varying times are shown in fig. 8.10. These results have been published elsewhere and show a complex microhardness-ageing time behaviour (ref. 92).

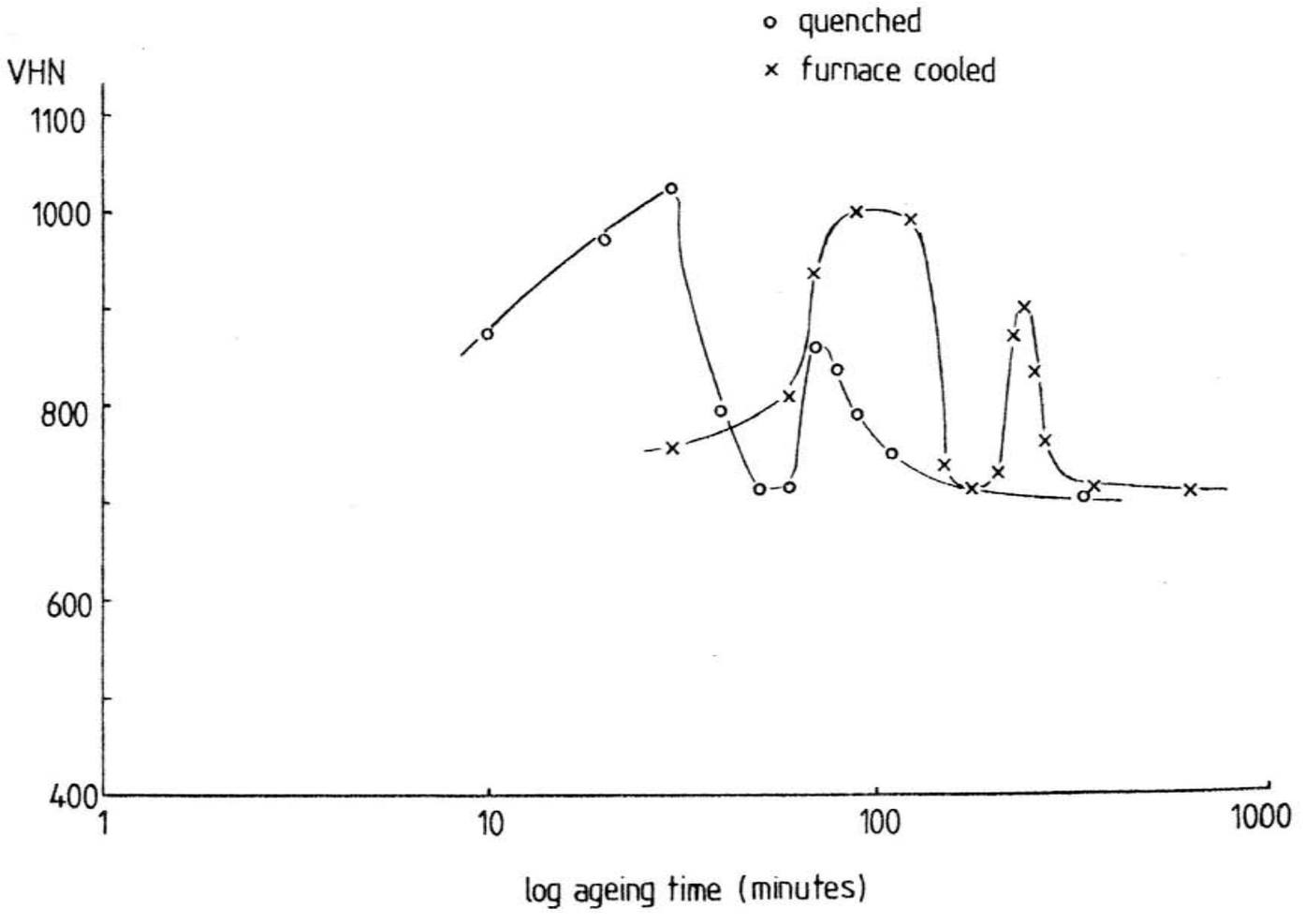

Fig. 8.10 Plots of microhardness versus log ageing time for bulk samples SST at 1100°C quenched or furnace cooled and then aged at 600°C.

Both the samples exhibit a two stage hardening variation with ageing time. The hardness against ageing time graph for the quenched specimen shows two hardness peaks at about 30 minutes and 70 minutes, with the peak hardness value of 1000 VHN occuring at 30 minutes. The furnace cooled sample shows a markedly different behaviour in that the peak hardness values occur at about 100 minutes and 245 minutes.

The behaviour of the two samples can be understood in terms of the role of vacancies and/or solubility excess in the ageing process. Thus on ageing at 600°C a precipitation process occurs, but the enhanced vacancy concentration and/or solubility excess present in the quenched alloy results in a much more rapid ageing process, so that the hardness maxima occurs at shorter ageing times than in the furnace cooled sample.

The presence of two hardness peaks after both the treatments could be due to a two stage hardening process involving metastable and stable precipitates and/or a solute redistribution in the matrix phase.

8.2.5 SEM Studies of the Powders Used in the Sintered Magnet Production

These studies were undertaken to compare the effects of the different powder production techniques on the particle size.

8.2.5a The Ball Milled Only Material

The secondary electron micrograph of the ball milled material (produced as detailed in section 6.3.2) is shown in fig. 8.11a with 10μm markers. It can be seen that the particle size varies from about 5μm to about 20μm. The surfaces of the particles are quite smooth compared

with the particle surfaces in the ball milled 2:17 material (see fig. 7.5a). This is possibly a consequence of the wet ball milling process used with the Nd-Fe-B alloy; the process is more effective as the material is broken up and is not compacted against the sides of the ball milling cylinder but is maintained in suspension in the liquid.

8.2.5b The Hydrogenated Only Powder Specimens

The secondary electron micrographs of the samples hydrogenated at 33 atm and 200 atm are shown in figs. 8.11b and 8.11c respectively. Comparing the two micrographs it can be clearly seen that the higher hydrogenation pressure has resulted in a smaller particle size and some cracking within the particles.

The surface condition of the particles show that they are highly brittle and clean. The particle size in the powder hydrogenated at 200 atm is about 20 μm to 40 μm in diameter. The particles appear also to be more flake-like than the BMO material and this is a consequence of intergranular decrepitation. This is illustrated at A in fig. 8.11c, where it appears that cracking has occurred at a matrix-Nd rich intergranular interface.

8.2.5c The Hydrogenated and then Ball Milled Powders

The secondary electron micrographs are shown in figs. 8.11d and 8.11e for the samples hydrogenated at 33 atm and 200 atm and then ball milled.

The particle size of the powder hydrogenated at 33 atm and then ball milled is in the range 10 μm to about 50 μm. The particle size

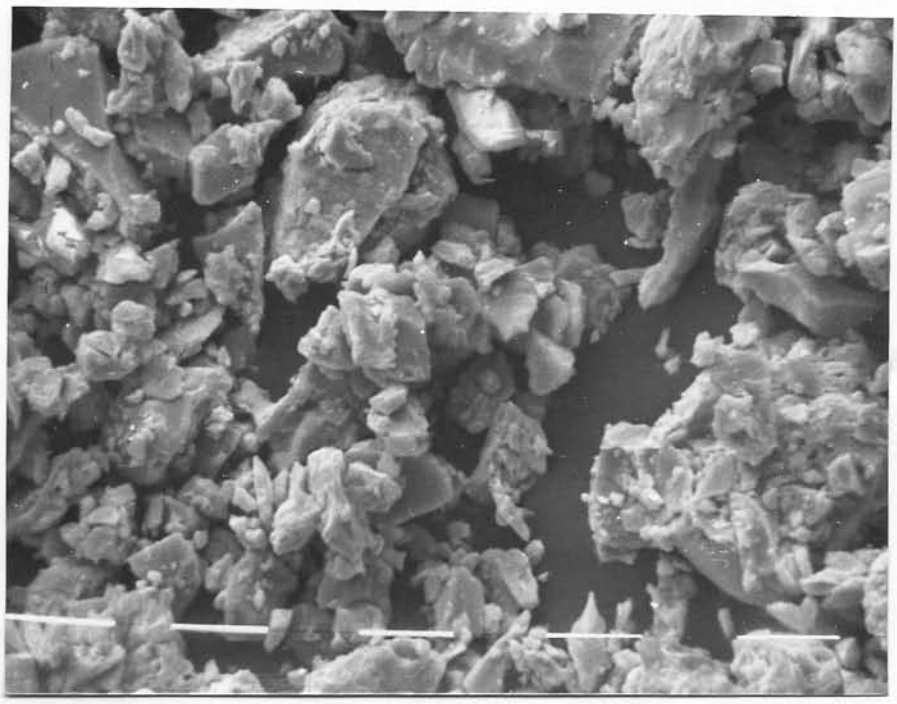

Fig. 8.11a Secondary SEM image of BMO Nd-Fe-B. (x 1250).

(10 μ markers).

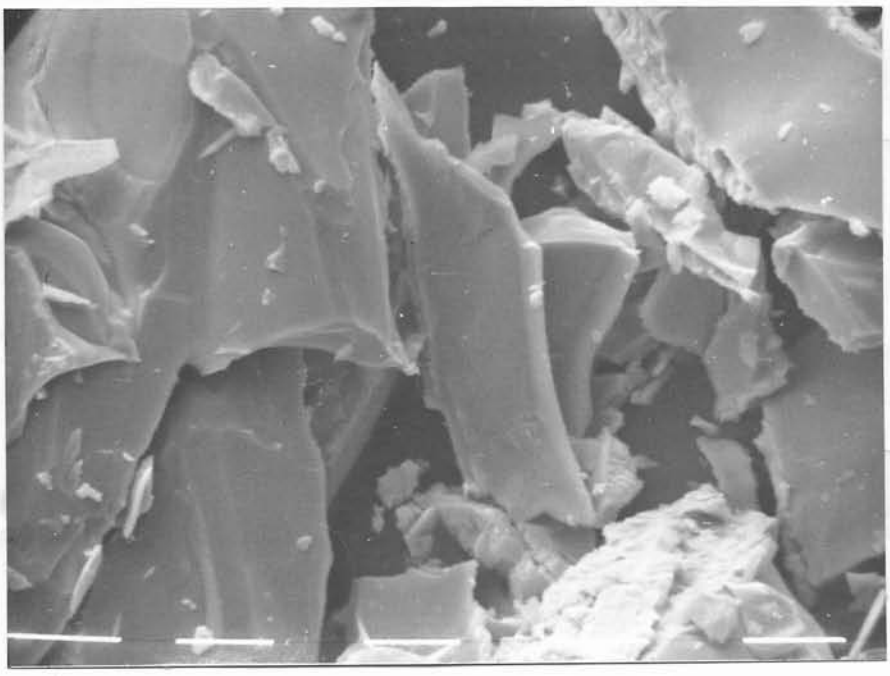

Fig. 8.11b Secondary image of hydrogenated at 33 atm Nd-Fe-B. (x 1250).

(10 μ markers).

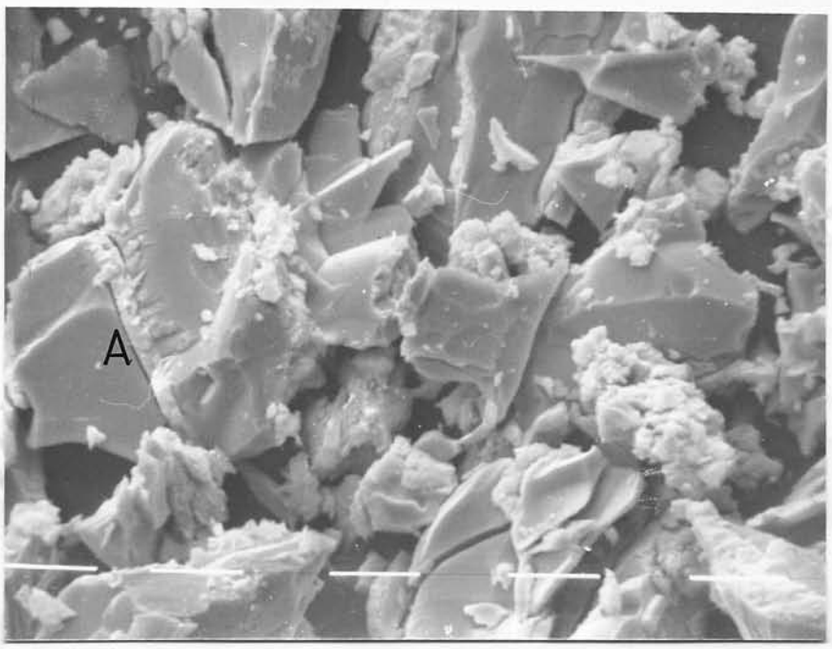

Fig. 8.11c Secondary SEM image of hydrogenated at 200 atm Nd-Fe-B. (x 1250). (10 μ markers).

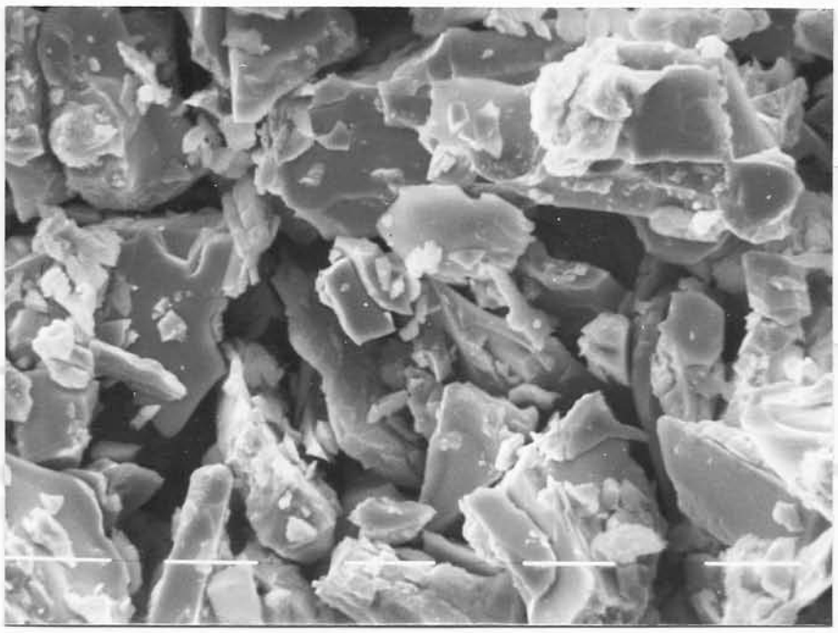

Fig. 8.11d Secondary SEM image of hydrogenated at 33 atm and then ball milled Nd-Fe-B. (x1250). (10 μ markers).

of the powder hydrogenated at 200 atm and then ball milled (see fig. 8.11e) is in the range 10 μm to about 40 μm. Thus, the higher hydrogenating pressure has an effect on the particle size. A smaller particle size is possible by using two methods:

1. Optimise the ball: material ratio during the ball milling operation.
2. Optimise the ball milling time.

In addition, an investigation is necessary to study whether exposure of the hydrogenated material to air has any large effect on the magnetic properties due to oxidation.

The particle sizes observed are in agreement with the densities measured on the sintered samples, and there is also an optimum particle size requirement for achieving the optimum magnetic properties.

8.3 Studies of the Sintered Specimens

8.3.1 Studies of the Magnetic Properties of the Sintered Specimens

8.3.1i The Magnetic Properties of the Samples Quenched or Furnace Cooled from 1100°C and then Aged at 600°C

The heat treatments given to these samples are described in section 6.5.3iiA. The plots of the intrinsic coercivity ${}_iH_c$ versus log ageing time for the quenched and slow cooled specimens are shown in fig. 8.12. The plots of the remanence, B_r, and energy product, BH_{max}, versus log ageing time for the two specimens are shown in fig. 8.13 and 8.14 respectively.

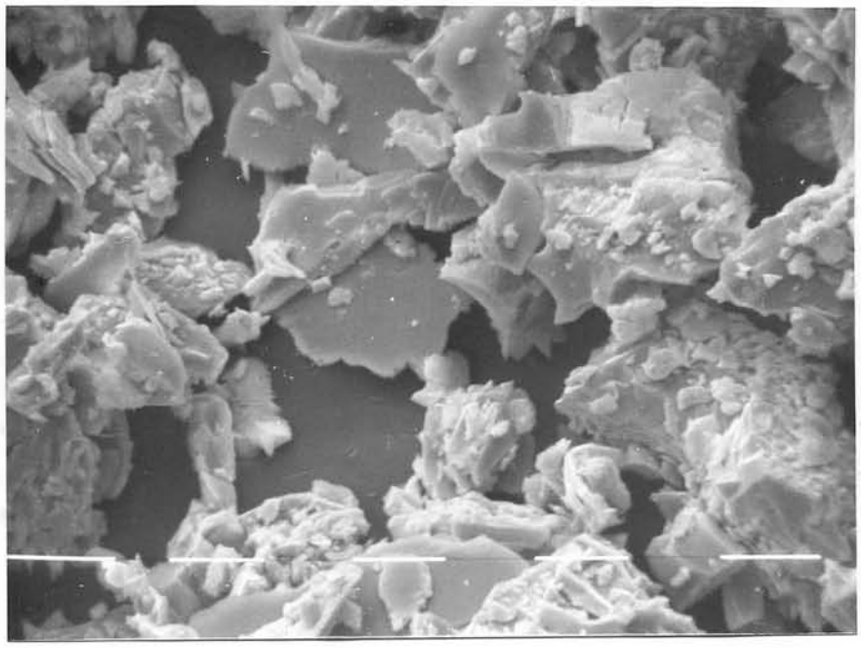

Fig. 8.11e Secondary SEM image of hydrogenated at 200 atm and then ball milled Nd-Fe-B. (x 1250). (10 μ markers).

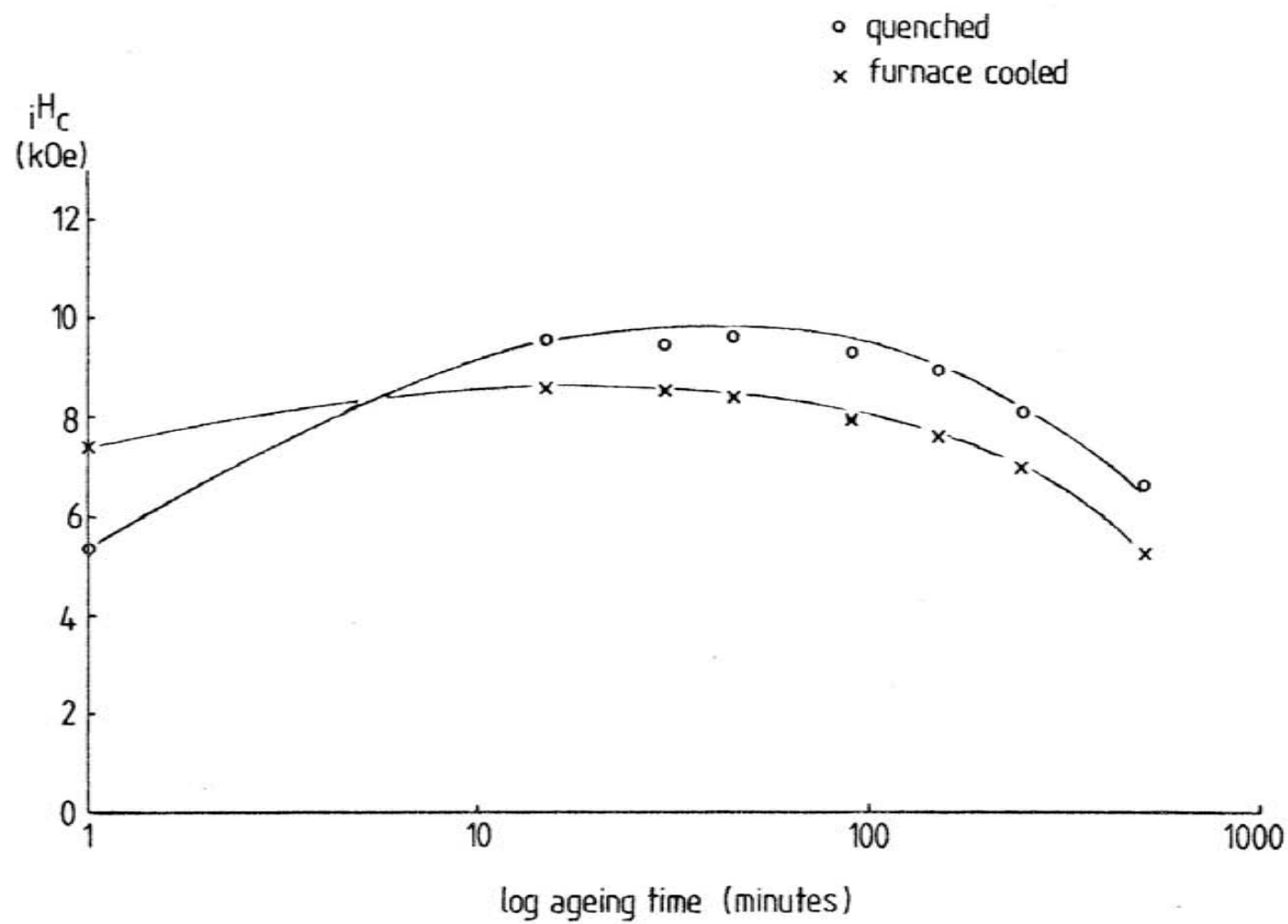

Fig. 8.12 Plots of $_iH_c$ versus log ageing time for sintered samples SST at 1100°C, quenched or furnace cooled and aged at 600°C.

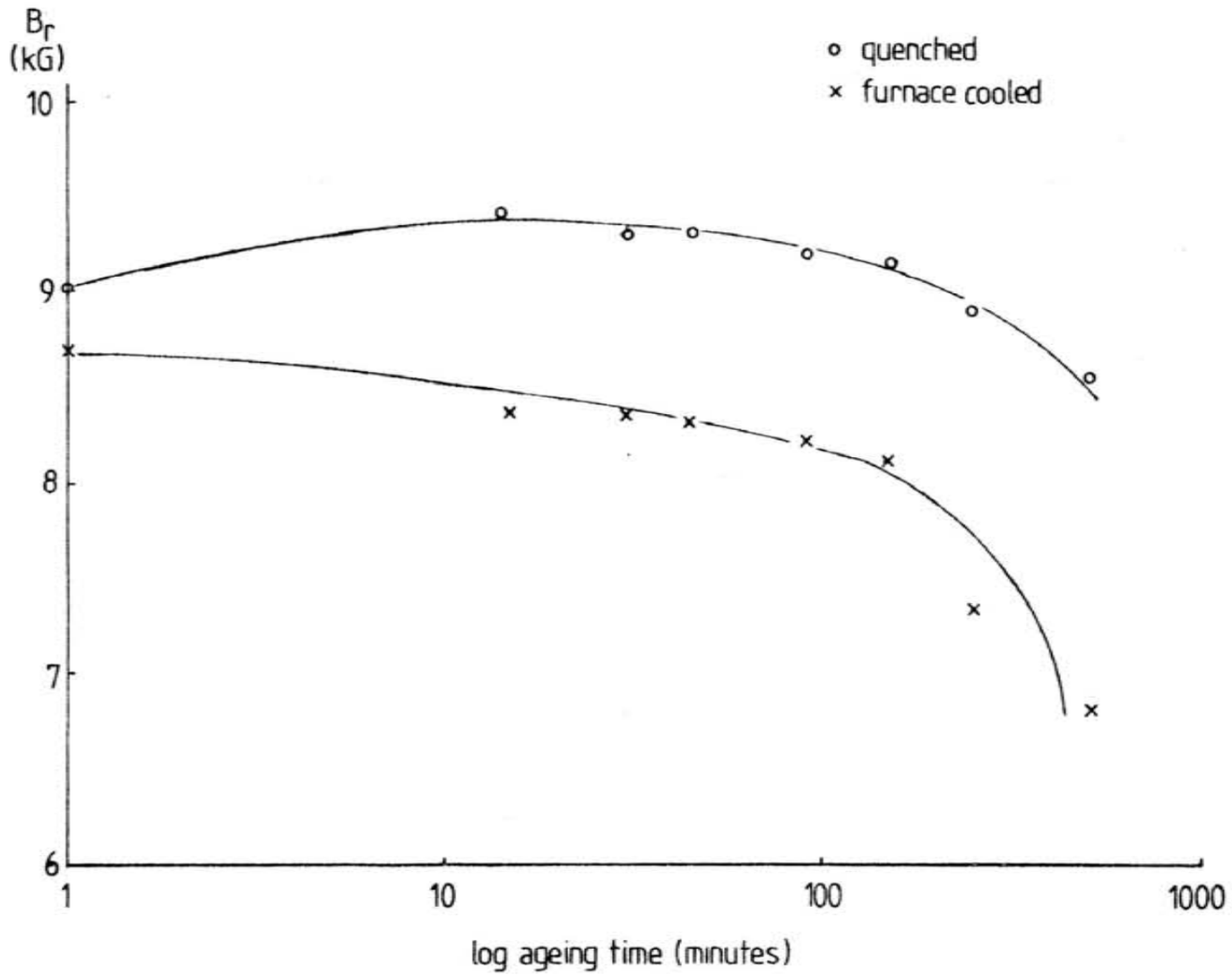

Fig. 8.13 Plots of B_r versus log ageing time for sintered samples SST at 1100°C, quenched or furnace cooled and aged at 600°C.

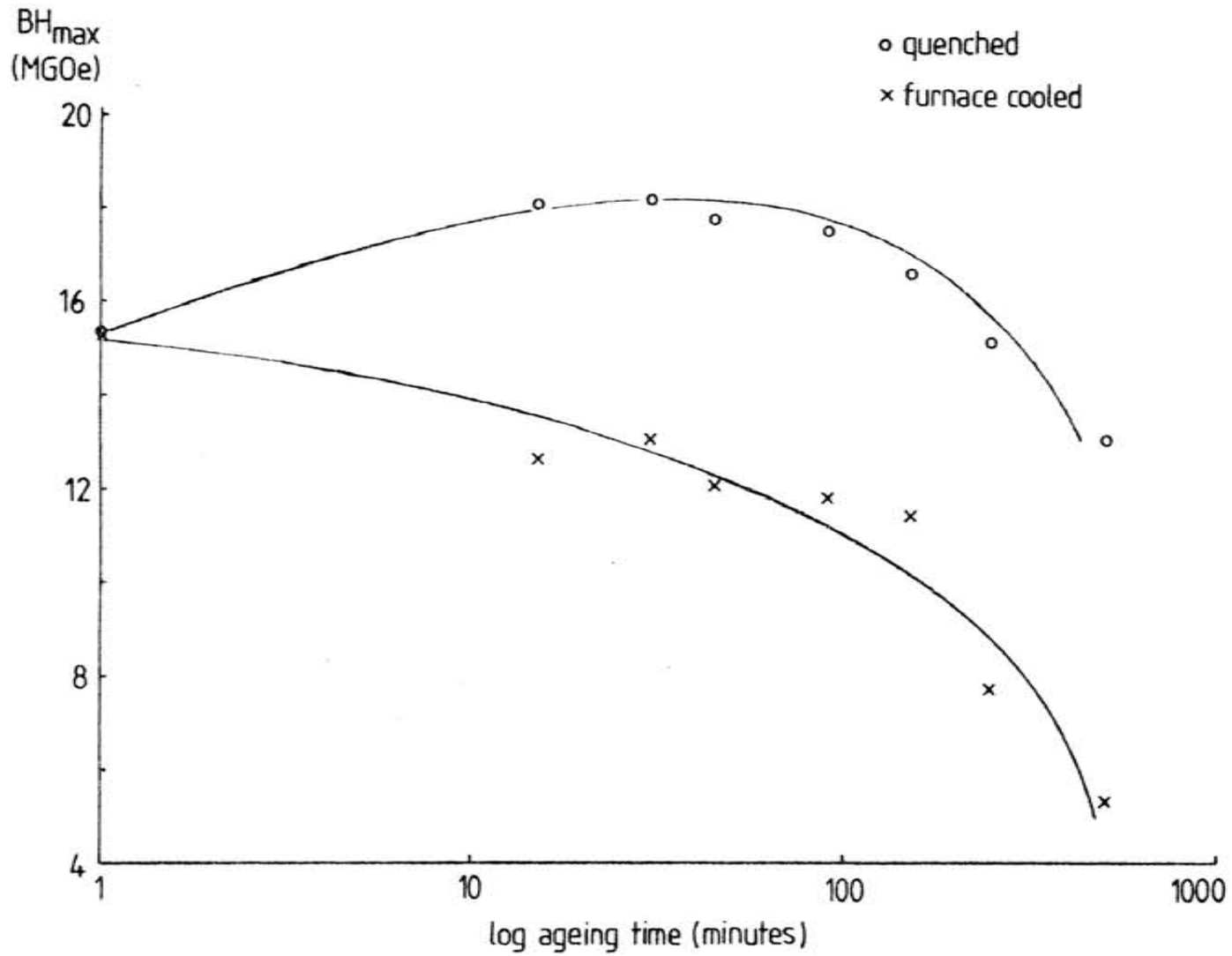

Fig. 8.14 Plots of BH_{max} versus log ageing time for sintered samples SST at 1100°C, quenched or furnace cooled and aged at 600°C.

The maximum ${}_iH_c$ value of about 9.6 kOe occurs for the quenched specimen, this value is maintained over a large ageing time range of about 15 minutes to 90 minutes.

The increases in the ${}_iH_c$ values on ageing at 600°C is possibly due to the growth of coherent precipitates. The initial rise in the ${}_iH_c$ values is greater for the quenched specimen and this can be explained by a solubility excess which leads to more rapid precipitate growth on ageing. This may be related to the inter-columnar phases observed in the bulk aged samples (see section 8.2.3).

The possible growth of precipitates or redistribution of solute atoms would act as sites for domain pinning as in the 2:17 alloys. This would explain the increase in ${}_iH_c$ on ageing and its subsequent fall. Ormerod (ref. 91) has shown that oxidation during processing results in the formation of an Fe-rich phase and a fall in ${}_iH_c$ to less than 200 Oe. This may also be a contributing factor in the variation of ${}_iH_c$ with annealing time. Previous investigators have observed a boron-rich $NdFe_4B_4$ phase in the sintered magnets (refs. 121, 122) or $Nd_2Fe_7B_6$ phase (ref. 118). Mishra et al. (ref. 122) suggested that on annealing the grain boundary chemistry is altered, so that reverse domain nucleation is more difficult. This has been linked to the presence of $NdFe_4B_4$ precipitates observed at grain boundaries in a transmission electron microscope.

The variations of B_r and BH_{max} with ageing time for the quenched specimen show a similar increase up to about 40 minutes (see figs. 8.13 and 8.14). However, the variations of B_r and BH_{max} for the furnace cooled sample both show a steady decrease up to about 90 minutes and then a large fall with increasing ageing time. This may be a result of a subtle difference in the initial condition of the microstructure in

the furnace cooled sample before annealing.

8.3.1ii The Intrinsic Coercivities of the Samples Quenced from 1100°C and then Aged at 540°C to 660°C

The heat treatments given on these samples are detailed in section 6.5.3iiA. The plots of $_iH_c$ versus log ageing time for the ageing temperatures 540°C-660°C are shown in fig. 8.15. As can be seen there is quite a wide variation in the behaviour of $_iH_c$ with log ageing time.

The sample aged at 540°C has been investigation by Hopkins (ref. 117). The intrinsic coercivity falls gradually up to an ageing time of about 10 minutes and then falls quickly to zero at around 30 minutes. The sample was re-solid solution treated at 1100°C for one hour and then quenched and aged for 30 minutes at 600°C. It was found that the $_iH_c$ value was about 9.5 kOe; it is therefore clear that some phase change or structural change occured on ageing at 540°C. The ageing temperature of 540°C is below the melting point of the Nd-rich phase (ref. 86): thus, this may explain the lack of development of the intrinsic coercivity in this specimen. The intrinsic coercivity may be dependent on the formation of a phase associated with the melting of the Nd-rich phase; this phase may not form on ageing at 540°C and thus a dislocation pinning coercivity mechanism does not occur.

The samples aged at 570°C and 630°C show a similar variation of $_iH_c$ with log ageing times. It appears that only at an ageing temperature of 600°C are there any developments in $_iH_c$ with ageing time. This could be due to the position of this alloy composition in the ternary Nd-Fe-B phase diagram, and any variations in temperature has a critical effect on the microstructure.

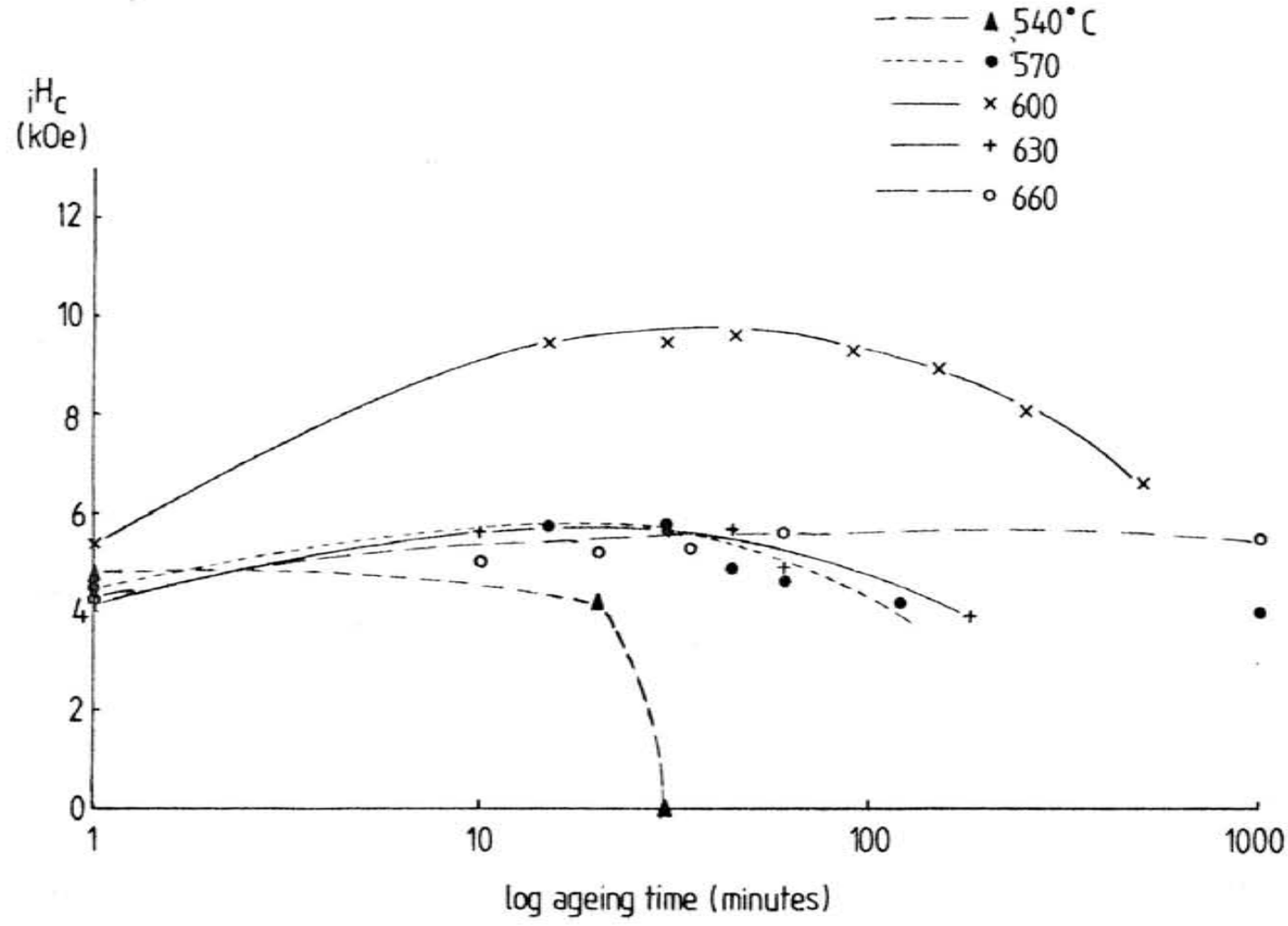

Fig. 8.15 Plots of $_iH_c$ versus log ageing time for sintered samples SST at 1100°C, quenched and aged at 540°C-660°C.

At an ageing temperature of 600°C, the $_iH_c$ values do not increase by a large amount with ageing time, and there is only a very broad peak in the $_iH_c$ versus ageing time variation.

8.3.1iii The Variation of Intrinsic Coercivity with Ageing Temperature

The plot of $_iH_c$ versus ageing temperature for the samples discussed in the previous section for an ageing time of about 40 minutes are shown in fig. 8.16.

These results agree quite well with Sagawa et al. (ref. 86) who showed a maximum $_iH_c$ value at an ageing temperature of between 870 and 930 K (600°C to 660°C). However, this investigation has found that the range of ageing temperatures corresponding to the peak $_iH_c$ value is smaller than that found by these workers.

8.3.2 The Magnetic Properties of the Sintered Magnets Produced from HD and then Ball Milled

Two sintered magnets were produced from powder that had been hydrogen decrepitated and then ball milled. Two HD pressures were used: 33 atm. and 200 atm. The procedure for making the powders is detailed in section 6.4.3.

Both the samples were quenched from 1100°C after one hour and then aged at 600°C. The variations of $_iH_c$, B_r and BH_{max} with log ageing

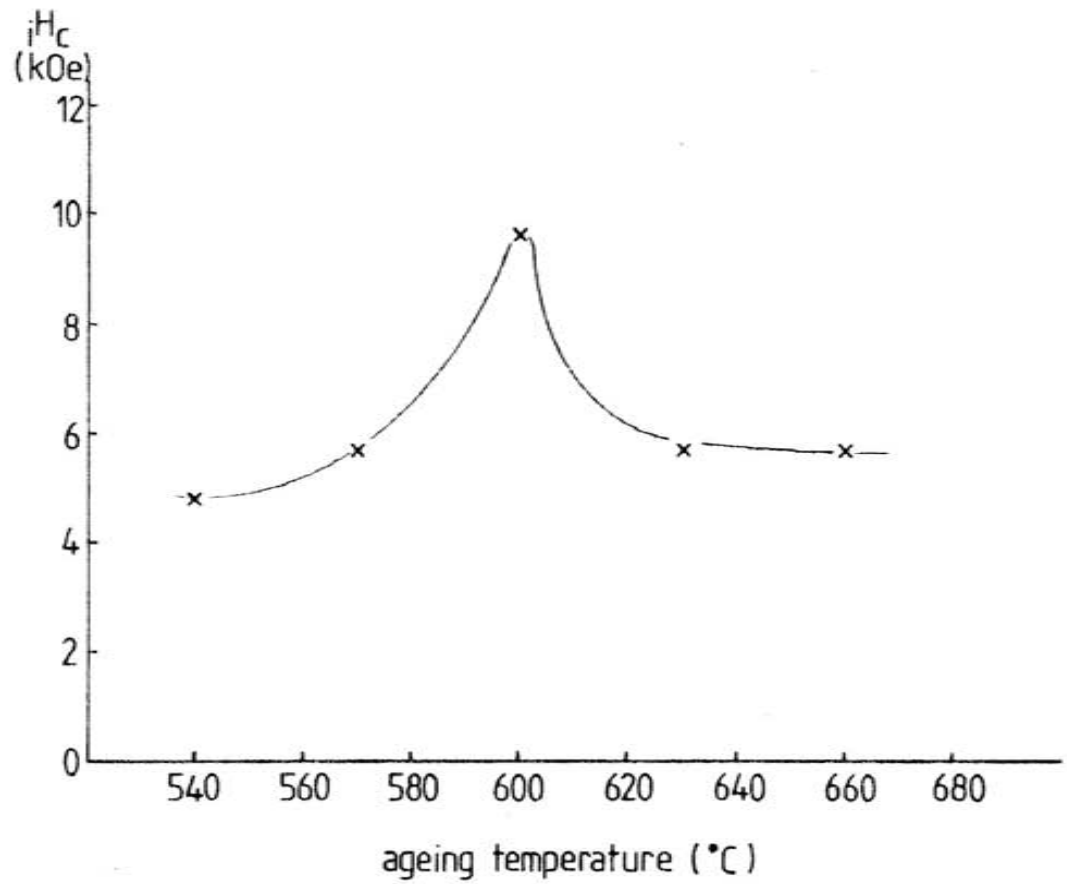

Fig. 8.16 Plot of maximum $_iH_c$ values versus ageing temperature for samples SST at 1100°C and quenched.

time for the samples produced from powder decrepitated at 33 atm. and 200 atm. are shown in figs. 8.17 and 8.18 respectively.

The magnetic properties of both the samples are lower than those produced from ball milled only (BMO) material. The maximum $_iH_c$ values of the two samples are about the same (approximately 5.5 kOe). However, the B_r and BH_{max} values for the sample HD at 200 atm. are higher than those for the sample HD at 33 atm. This may be attributed to a smaller particle size in the first sample which leads to an increased density on heating at 1100°C. The smaller particle size may arise from a more extensive intragranular cracking process rather than just a grain boundary cracking process (ref. 98), due to the higher hydrogen pressures.

The lower coercivity values in the HD specimens compared with the BMO specimens may be explained in terms of the coercivity mechanism in the NdFeB alloys. Croat (ref. 81) has shown in melt-spun materials that as the crystallite size increases, the coercivity decreases. Thus, only for a certain particle size is the $_iH_c$ an optimum, this was suggested to be the single domain particle size. However in these alloys it is still not fully understood whether the coercivity is nucleation (single domain) controlled or precipitation controlled (ref. 123), or a combination of both these factors.

Another explanation for the lower coercivity values is that after hydrogen decrepitation, the exposure of the highly clean friable surfaces to the atmosphere leads to a rapid oxidation of these surfaces, which is consequently detrimental to the intrinsic coercivity. As with

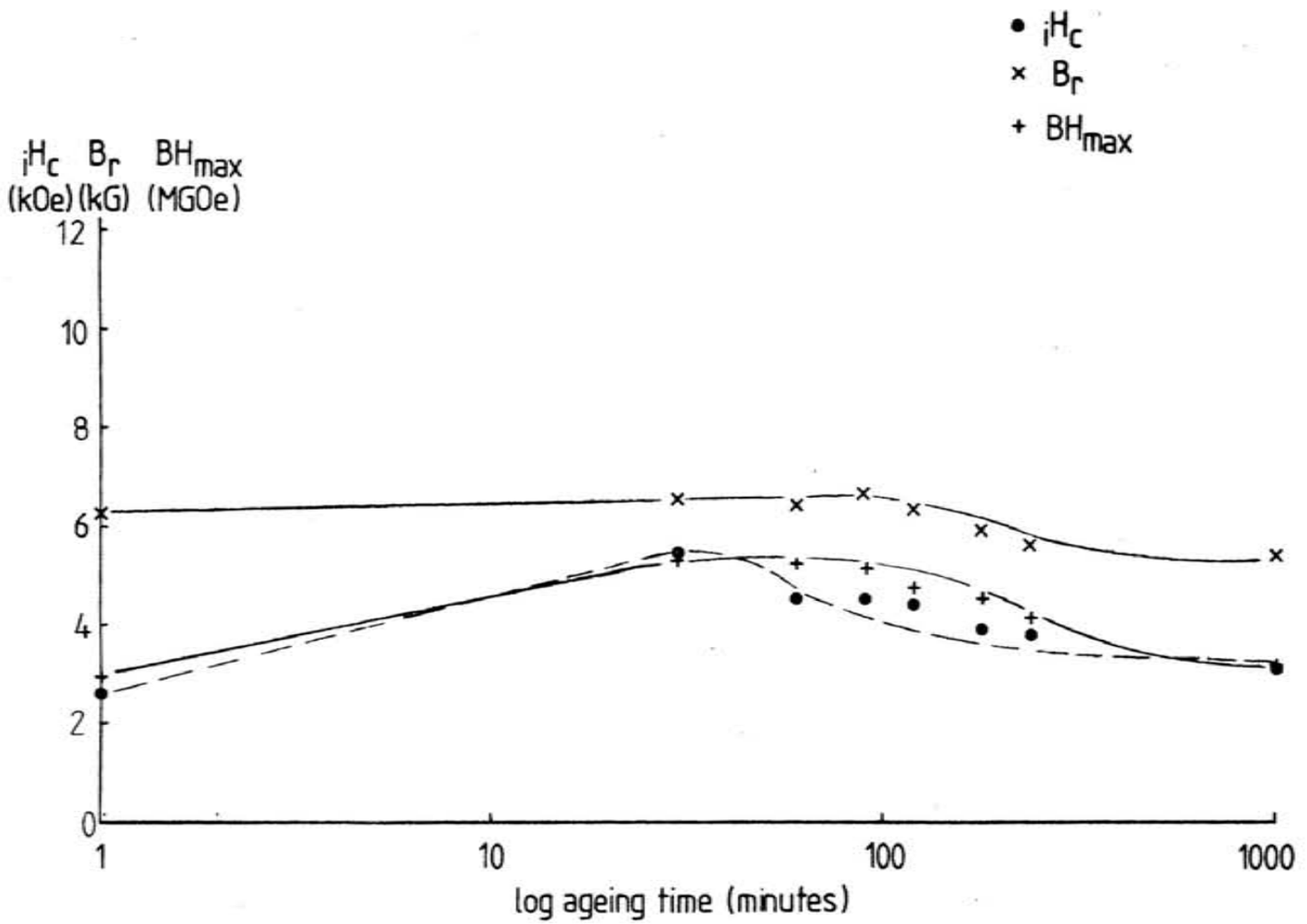

Fig. 8.17 Plots of magnetic properties versus log ageing time for sintered HD at 33 atm sample, SST at 1100°C, quenched and aged at 600°C.

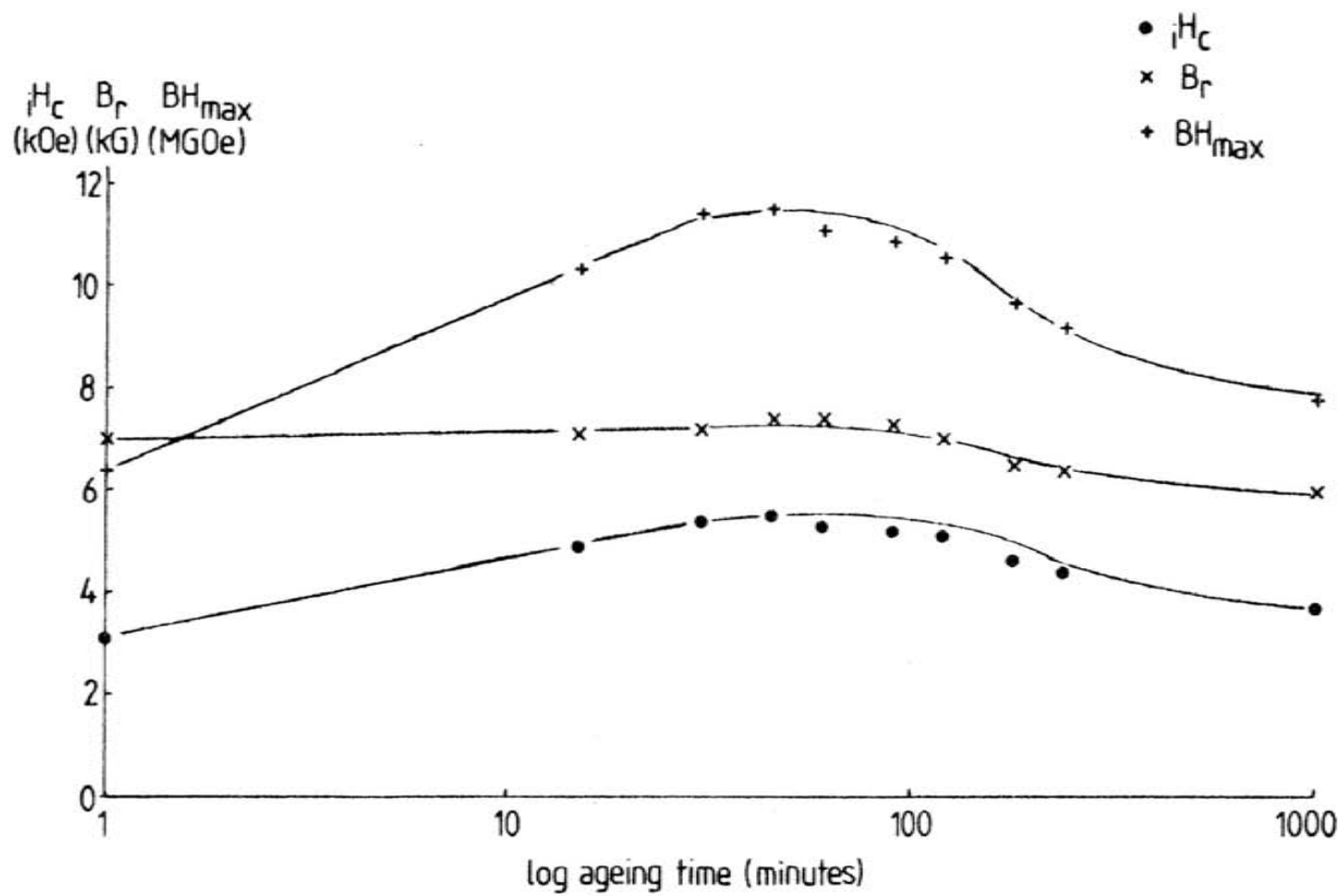

Fig. 8.18 Plots of magnetic properties versus log ageing time for sintered sample HD at 20 atm SST at 1100°C, quenched and aged at 600°C.

the 2:17-type alloy, a further study is required to achieve the optimum hydrogenation and ball milling conditions in the NdFeB alloy.

8.3.3 Density Measurements

The densities of the bulk sample, the sintered magnet produced from BMO material and the two samples produced via HD at 33 atm and 200 atm and then ball milled are shown in table 8.2.

table 8.2

Table of densities for the NdFeB alloy

Sample	Density (Kgm^{-3})
bulk alloy	7.2
sintered magnet from ball milled material	7.1
sintered magnet (HD at 33 atm)	6.6
sintered magnet (HD at 200 atm)	6.7

The density of the sintered magnet produced from ball milled only material is lower than the density achieved by Sagawa et al. (ref. 86); this is attributed to the smaller particle size achieved by Sagawa.

The HD sintered magnets have lower densities than the sintered magnet produced from ball milled only material and this is consistent with the lower B_r and BH_{max} values of these samples. The density of the sample HD at 200 atm is slightly higher than the one HD at 33 atm. and these results further support the importance of particle size in achieving high remanences and energy products.

8.3.4 Degassing Studies on the Hydrogenated NdFeB Alloy

A previous study has shown that when the NdFeB alloy is hydrogen decrepitated, there is an expansion of the $Nd_2Fe_{14}B$ matrix phase (ref. 98). Due to oxidation of the powder in the degassing apparatus, it was difficult to obtain a quantitative value of the amount of hydrogen absorbed. However, it has been shown (ref. 98) that hydrogen is desorbed at two temperatures: about 250°C and 500°C. The first degassing temperature may be attributed to the loss of hydrogen from the matrix phase as this is where the hydrogen decrepitation process is the most rigorous. This is followed by a further loss of hydrogen from the Nd-rich intergranular phase at about 500°C. Fruchart et al. (ref. 124) concluded that hydrogen entered into the sites that had RE nearest neighbours and that up to 5.2 hydrogen atoms could be absorbed per unit cell.

8.3.5 Microhardness Studies of the Sintered Alloy

Microhardness studies were made on the sintered samples detailed in sections 8.3.1i and 8.3.1ii. The studies were made to see if a correlation exists between a rise in microhardness on ageing and a rise in coercivity on ageing. This has been shown to be true in the case of the 2:17 alloy where an excellent correlation has been found between the microhardness and intrinsic coercivity on ageing (refs. 66, 67). This correlation was evidence of the part played by coherent precipitates in pinning both dislocations and domains.

8.3.5i Microhardness Studies on the Samples Quenched or Furnace Cooled from 1100°C and then aged

The heat treatments of the two samples are detailed in section 6.5.3iiA. The plots of microhardness versus log ageing time are shown in fig. 8.19. It can be seen that unlike the bulk specimens (see fig. 8.11) the quenched and furnace cooled specimens both exhibit two microhardness peaks at approximately the same ageing times. (40 minutes and 150 minutes). This may be attributed to the similar small grain size in both these specimens which leads to similar diffusion distances. The peaks in microhardness are approximately concurrent with the broad peaks in the intrinsic coercivity of these samples (see fig. 8.12). This may suggest that on ageing some chemical change occurs in the matrix phase, which is possibly related to the growth of metastable coherent precipitates which pin domains and dislocations, or alternatively due to solute redistribution.

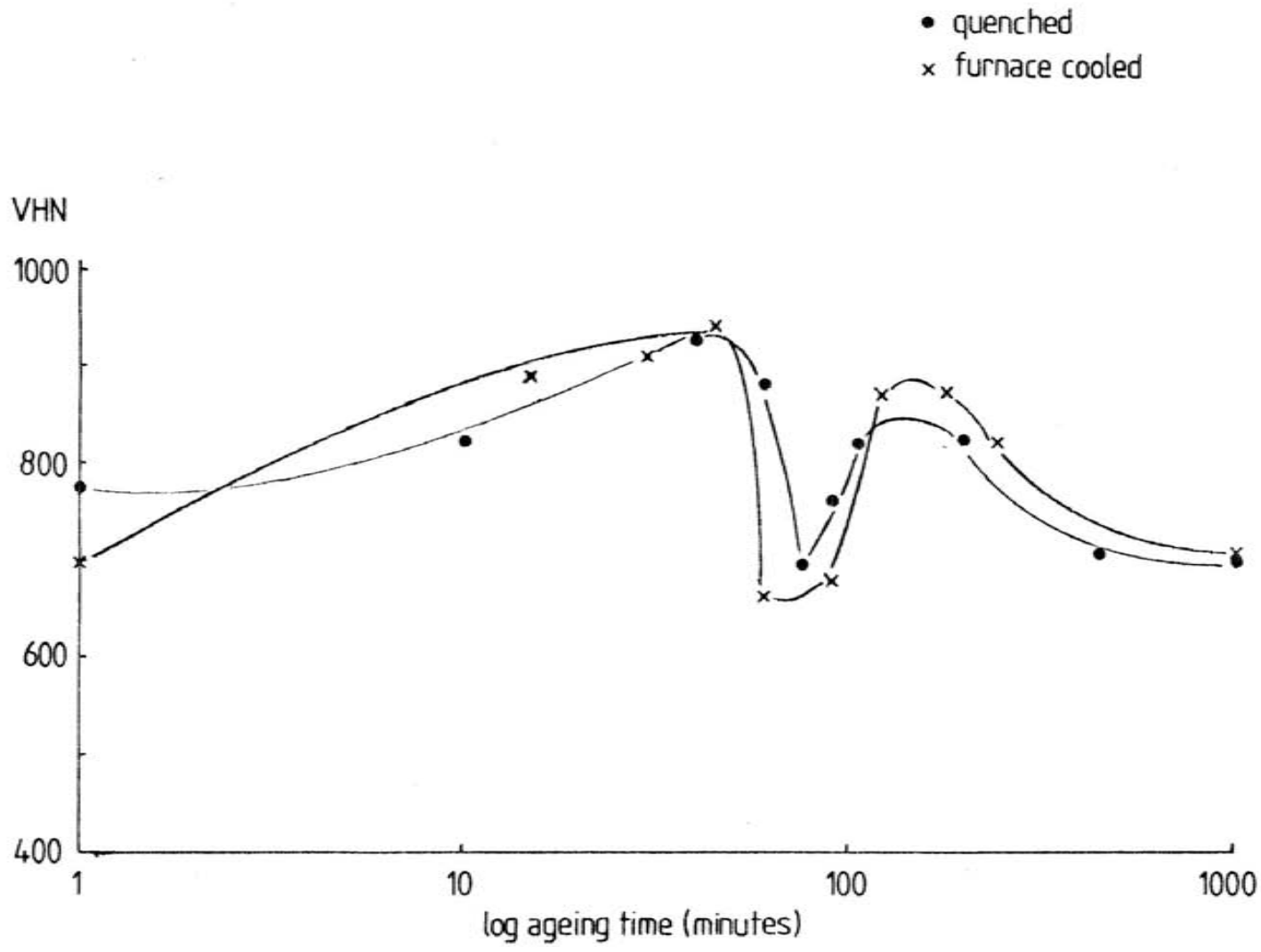

Fig. 8.19 Plots of microhardness versus log ageing time for sintered samples SST at 1100°C quenched or furnace cooled and aged at 600°C.

A number of workers have observed a b.c.c. platelet phase at grain boundaries in "As sintered" magnets. This phase becomes "smooth" and lines the grain boundaries on ageing. Thus it was proposed that the ageing treatment, rather than producing coherent precipitates, merely removes sites of reverse nucleation (refs. 118,125). Hadjipanayis (ref. 121) has proposed that grain boundary pinning is responsible for the coercivity mechanism. It is clear that much more detailed transmission electron microscopy work is required in this alloy, particularly on the $Nd_2Fe_{14}B$ phase to see if there are any lattice faults associated with a coherent precipitate phase.

It is important to establish that the broad peak in coercivity on ageing is not a result of oxidation due to successive heat treatments. Thus, after the ageing treatment, the samples were re-solid solution treated at 1100°C and then aged at 600°C for about 30 minutes and the intrinsic coercivity was recovered. Irreversible effects would be anticipated with oxidation.

8.3.5ii Microhardness Studies on the Samples Quenched from 1100°C and then Aged at 540°C-660°C

The heat treatments made on these samples are detailed in section 6.5.3iiA. The plots of the microhardness versus log ageing time are shown in fig. 8.20.

The microhardness of the sample aged at 540°C shows a small and steady decrease with ageing time. This is in marked contrast to the behaviour at 600°C and correlates with the fall in $_iH_c$ with ageing time (see fig. 8.15) at 540°C.

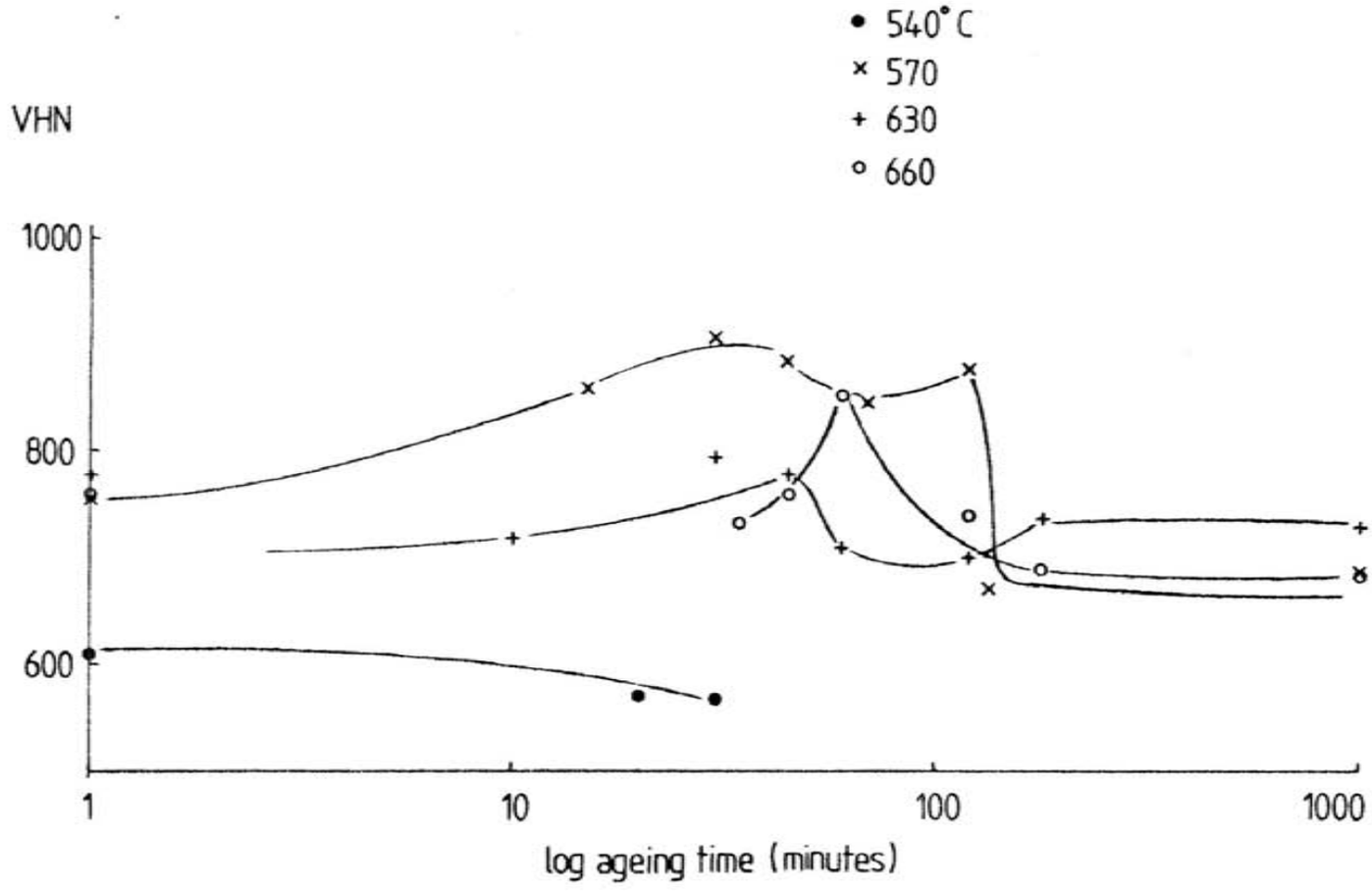

Fig. 8.20 Plots of microhardness versus log ageing time for sintered samples SST at 1100°C, quenched and aged at 540°C-660°C.

The sample aged at 570°C shows a two stage hardening phenomenon, with maxima occurring at about 30 minutes and 120 minutes. However, there is less of a fall in the microhardness after the first peak compared with the sample aged at 600°C (see fig. 8.19). This is also the case for the sample aged at 630°C, and the second maxima occurs at about 180 minutes. In addition, the sample aged at 660°C shows only one microhardness peak at about 60 minutes.

It appears that at the ageing temperatures above and below 600°C, different phase changes occur, which alters the intrinsic coercivity and microhardness on ageing to different extents. The ageing phenomenon appears to be much more complex than in the case of the 2:17 type alloy discussed in the previous chapter where there is a clear correlation between the peak hardness and peak ${}_iH_c$ values.

8.3.6 Optical Metallography of the Sintered Samples

Due to the dense microstructure in the sintered samples, the polishing techniques used produced better micrographs than in the case of the 2:17 alloy sintered specimens. Since the lack of porosity allowed flatter surfaces to be achieved on grinding. The microstructures of the samples produced from BMO after different heat treatments were all found to be similar. However, there was an increase in the amount of porosity in the specimens produced from hydrogenated material.

8.3.6.i The Specimen Quenched from 1100°C and then Aged at 600°C

The optical micrograph of this specimen is shown in fig. 8.21. Two phases can be observed:

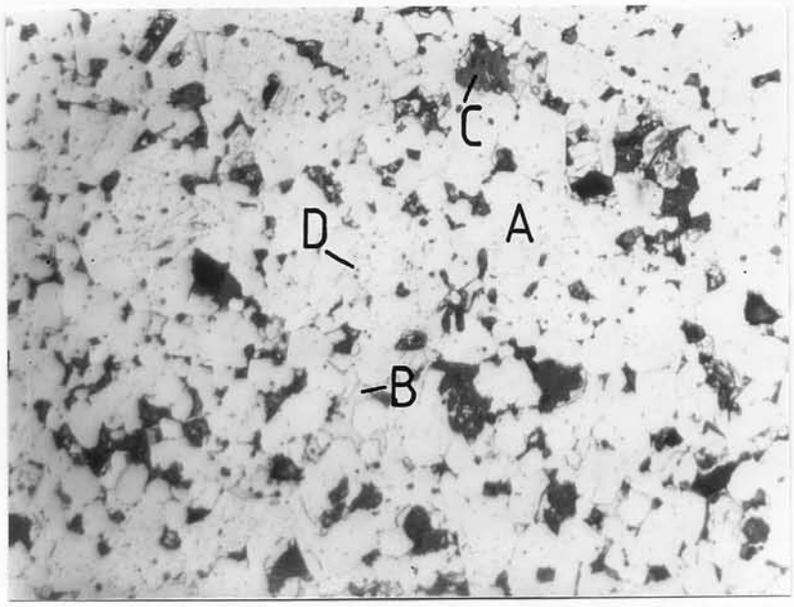

Fig. 8.21 Optical micrograph of specimen quenched from 1100°C and aged at 600°C for 80 hours. (x 400).

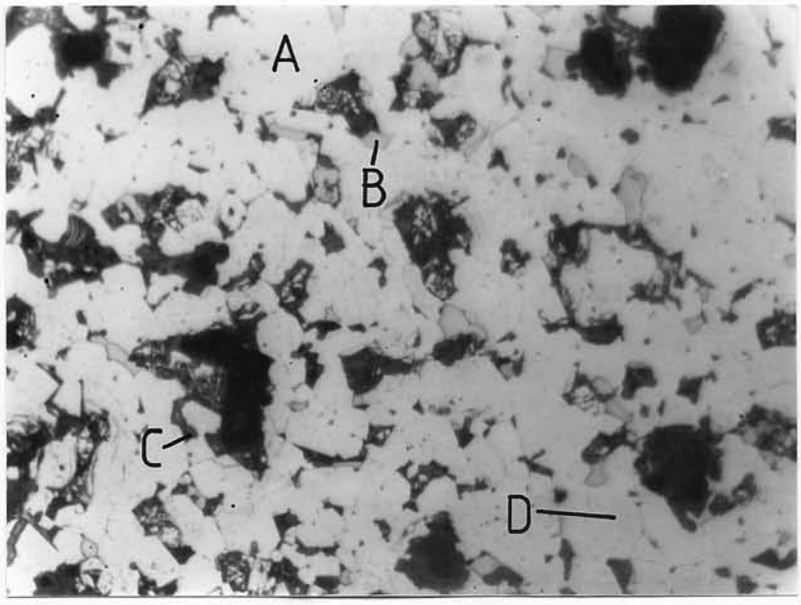

Fig. 8.22 Optical micrograph of sintered HD sample pressurised at 33 atm, quenched from 1100°C and aged at 600°C for 80 hours. (x 400).

1. A matrix phase (A).
2. An intergranular phase (B).

There is also possibility of a third phase that has been observed by a number of workers (refs. 91, 118, 121, 126) which is associated with the intergranular phase. This phase was found to be boron rich and of composition $NdFe_4B_4$. In fig. 8.21, there are some dark grey regions (C) which may be this third phase. The black regions are either "pull-out" of the phase (B) and (C) or porosity. Due to the high density of this sample (about 98%), the majority of the black regions must be "pull-out" and not porosity.

The intergranular phase B is a low melting point Nd-rich phase and during the sintering process is liquid (ref. 86). This phase therefore enhances densification and thus the high densities achieved in this alloy are the result. However, as this intergranular phase is Nd-rich, there may be problems with oxidation and corrosion of the highly reactive rare earth.

The matrix phase consists of the tetragonal $Nd_2Fe_{14}B$ composition: this is the phase responsible for the good magnetic properties due to the high magnetocrystalline anisotropy along the c-axis (ref. 86).

The small points scattered within the grains (D) have been found to be a fourth phase (see EDAX results in section 8.3.8) and are discussed later.

These four phases were observed in all the sintered specimens produced from BMO material. There was no evidence of large grain growth in these samples as occured in the bulk samples. This could be due to the much smaller initial grain size.

There was no evidence of a solid state precipitation process which correlates with the variations in $_iH_c$ and microhardness.

These results are similar to those obtained by Ormerod (ref. 91), and a comparison is given below in table 8.3.

table 8.3 Results of optical metallography on a BMO sintered sample.

Phase observed		Phase observed (ref. 91)
Matrix phase	(A)	Matrix phase 27 wt.% Nd
Intergranular phase	(B)	Grain boundary Nd-rich phase 80 wt.% Nd
Dark Grey phase	(C)	Boron-rich phase 28 wt.% Nd
Phase within grains	(D)	

8.3.6ii The Specimens Produced from Hydrogen Decrepitated and Ball Milled Material

As discussed in section 8.3.2, two sintered samples were produced from HD powder decrepitated at 33 atm. and 200 atm. Both the samples were quenched from 1100°C after one hour and then aged at 600°C.

The optical micrographs are shown in figs. 8.22 and 8.23 for the samples pressurised at 33 atm and 200 atm respectively. In both the micrographs four phases can be seen:

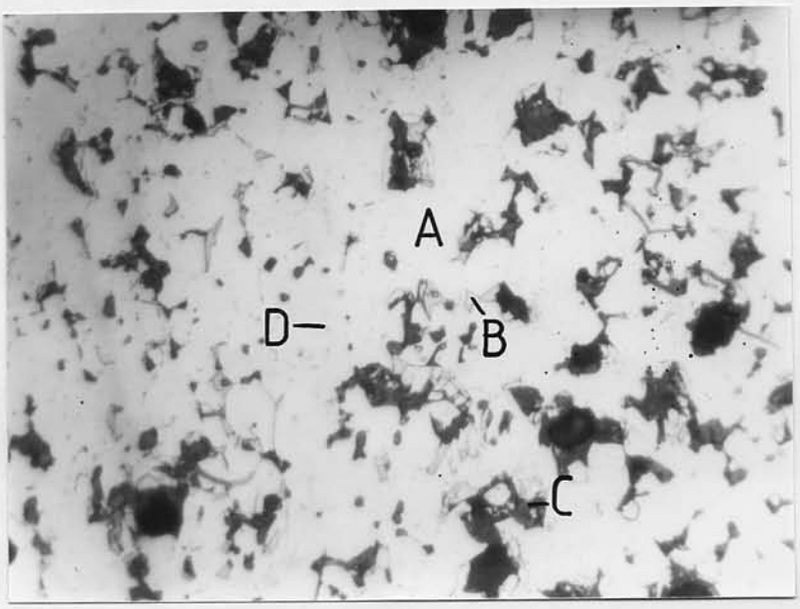

Fig. 8.23 Optical micrograph of sintered HD sample pressurised at 200 atm, SST at 1100°C and aged at 600°C for 80 hours. (x 400).

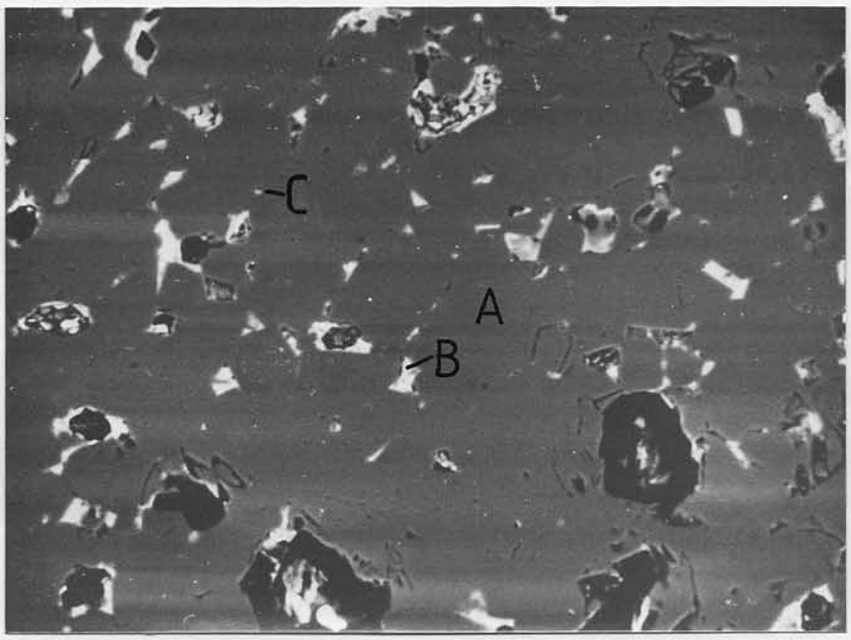

Fig. 8.24 Backscattered SEM micrograph of sample SST at 1100°C, quenched and aged at 570°C. (x 640).

1. A matrix phase (A).
2. A intergranular phase (B).
3. A dark grey phase (C).
4. A phase within the grains (D).

For the sample HD at 33 atm. (see fig. 8.22) there are large regions of porosity which is consistent with the low density values of this sample. This porosity is less extensive in the sample HD at 200 atm. and this is reflected in the slightly higher density value compared with the sample HD at 33 atm. The grain size in both these samples is larger than in the sample shown in fig. 8.21. This may explain the lower coercivity values observed in the samples produced via hydrogenation, in terms of a grain boundary pinning coercivity mechanism. However, the microhardness and intrinsic coercivity variations with ageing time imply that there is some domain pinning occurring. Thus, the coercivity mechanism is possibly a combined domain nucleation and domain pinning process.

8.3.7 SEM Studies of the Sintered NdBeB Alloy

The three samples quenched from 1100°C after one hour and then aged at 570°C, 600°C, 630°C and 660°C were studied in the electron microscope. This was to obtain information about any phase or composition changes on ageing that could be correlated with magnetic properties.

The backscattered electron micrographs of the specimens aged at 570°C, 600°C, 630°C and 660°C are shown in figures 8.24, 8.25, 8.26 and 8.27 respectively.

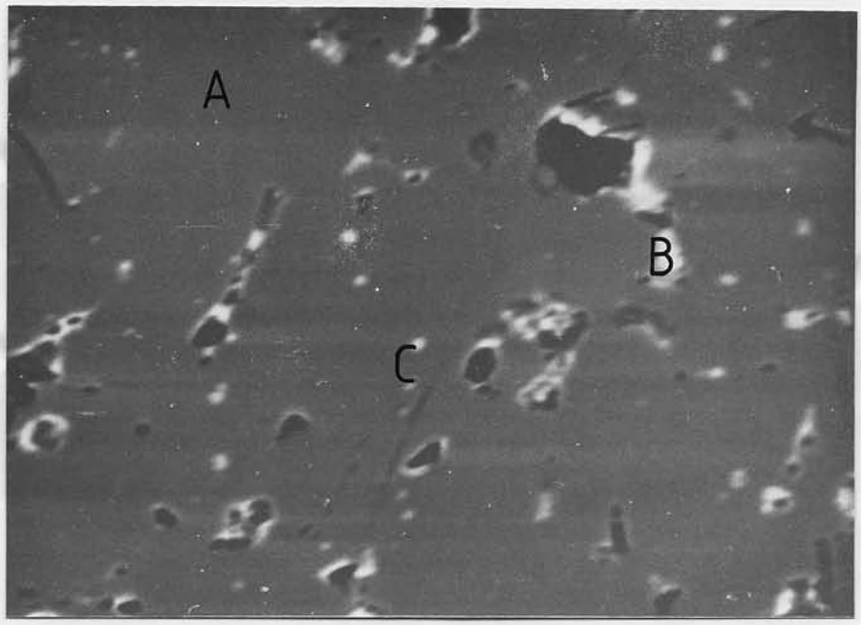

Fig. 8.25 Backscattered SEM micrograph of sample SST at 1100°C, quenched and aged at 600°C for 80 hours. (x 640).

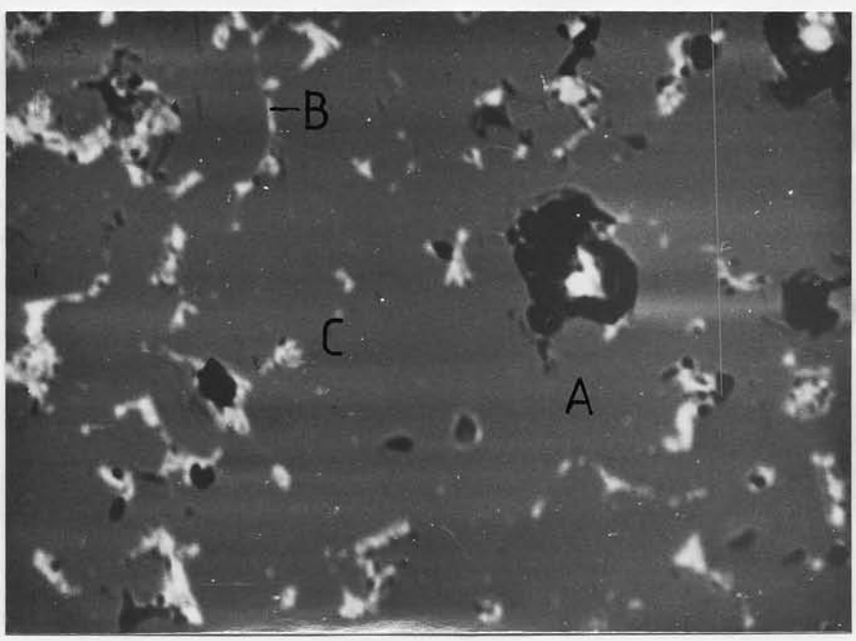

Fig. 8.26 Backscattered SEM micrograph of sample SST at 1100°C, quenched and aged at 630°C. (x 640).

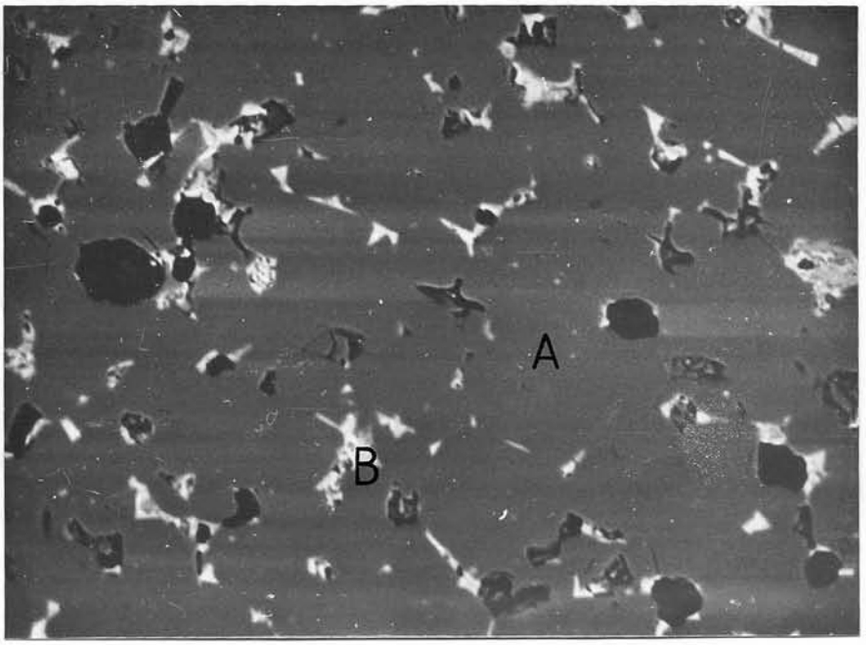

Fig. 8.27 Backscattered SEM micrograph of specimen SST at 1100°C, quenched and aged at 660°C. (x 640).

The samples aged at 570°C, 600°C and 630°C all show evidence of three phases:

1. A matrix phase (A).
2. An intergranular phase (B).
3. A light phase within the grains (C).

The matrix phase according to the literature (refs. 91, 118, 121) is the tetragonal $Nd_2Fe_{14}B$ phase and the intergranular phase is a Nd-rich phase. Ormerod (ref. 91) has shown that there is also a boron rich-phase associated with the intergranular regions. However, this was not observed due to the poor image contrast in these specimens. The optical micrographs (see section 8.3.6i) do show however the presence of a phase associated with the intergranular phase (see (C) in fig. 8.21) and this may be the boron rich phase.

The EDAX studies detailed in the next section have shown the light phase within the grains (see (C) in figs. 8.24, 8.25 and 8.26) to have a consistent composition which is richer in Fe. This light phase was not observed in the specimen aged at 660°C however. Thus, it would appear that there is some microstructure change on ageing at 660°C.

8.3.8 X-ray Microanalysis (EDAX) Studies of the Sintered Specimens

The sintered samples quenched from 1100°C and then aged at 570°C, 600°C, 630°C and 660°C for over 80 hours were investigated using X-ray microanalysis. The boron composition could not be detected with the equipment available so the substitution composition is given as x, an unknown.

The results of the EDAX investigations are given in table 8.4 (the at.wt. errors were in the range ±0.3 - ±0.5). The composition of the matrix phase in the samples aged at 570°C to 630°C is $NdFe_{6.2}B_x$. This composition is different to the $Nd_2Fe_{14}B$ composition observed by other workers (refs. 118, 121), but may be a result of the errors involved in the analyses. The matrix phase composition of the sample aged at 660°C is $NdFe_{6.7}B_x$ which is in better agreement with the composition observed elsewhere, (refs. 118, 121).

The composition of the Nd-rich intergranular phase is about $Nd_{3.4}FeB_x$, for the samples aged at 570°C and 600°C. This changes to $Nd_{3.1}FeB_x$ for the sample aged at 630 °C. These compositions are lower in Nd than the intergranular phase observed in the bulk material and may be the result of some Nd loss due to oxidation. At an ageing temperature of 660°C, the composition is $Nd_{2.7}FeB_x$. Thus, on increasing ageing temperature the composition of the intergranular phase becomes richer in Fe (and possibly boron) which may be concurrent with the disappearance of the phase (C) within the grains.

The phase observed within the grains (C) has the composition $NdFe_4B_x$ in the samples aged at 570°C and 600°C. This phase has been observed principally at grain boundaries, and has been associated with the Nd-rich phase (B) (see for example ref. 91). It has been shown to have the composition $NdFe_4B_4$. It is likely then that this is the same phase observed within the grains as isolated particles.

On ageing at 630°C, the composition of this phase is $NdFe_{2.2}B_x$, and ageing at 660°C causes the phase not to be present in the microstructure.

table 8.4 EDAX results for the sintered NdFe-B specimens

Heat treatment	Area details		Substitution composition (±0.3-0.5)
S.S.T. at 1100°C, quenched	Matrix phase	(A)	$NdFe_{6.2}B_x$
and aged at 570°C for 80 hours	Intergranular phase	(B)	$Nd_{3.4}FeB_x$
(see fig. 8.24)	Phase within grains	(C)	$NdFe_4B_x$
S.S.T. at 1100°C, quenched	Matrix phase	(A)	$NdFe_{6.2}B_x$
and aged at 600°C for 80 hours	Intergranular phase	(B)	$Nd_{3.4}FeB_x$
(see fig. 8.25).	Phase within grains	(C)	$NdFe_4B_x$
S.S.T. at 1100°C, quenched	Matrix phase	(A)	$NdFe_{6.2}B_x$
and aged at 630° C for 80 hours	Intergranular phase	(B)	$Nd_{3.1}FeB_x$
(see fig. 8.26).	Phase within grains	(C)	$NdFe_{2.2}B_x$
S.S.T. at 1100°C, quenched	Matrix phase	(A)	$NdFe_{6.7}B_x$
and aged at 660°C for 80 hours	Intergranular phase	(B)	$Nd_{2.7}FeB_x$
(see fig. 8.27).			

In terms of the magnetic properties, it is possible that the $NdFe_4B_x$ phase is necessary to achieve good magnetic properties. On ageing at too high temperatures causes this phase to disappear; which could be the reason for the poor magnetic properties. The growth of this phase may also be the cause of the variations of the microhardness and intrinsic coercivity with ageing time. Despite a number of attempts the $NdFe_4B_4$ phase could not be detected at the intergranular regions, and this may be a consequence of "pull-out" of the phase on polishing or the spread of the electron beam during X-ray microanalyses.

8.4 Summary

The results of the investigations on the Nd-Fe-B alloy can be summarised as follows:

1. The bulk "as cast" material consisted of three phases:
   a. a matrix phase of composition $Nd_2Fe_{14}B_x$.
   b. a Nd-rich intergranular phase.
   c. free Fe.

2. On S.S.T. at 1100°C the free Fe phase disappeared.

3. On ageing at 600°C (after S.S.T. at 1100°C) and then quenching the bulk material consisted of three phases:
   a. a matrix phase of composition $Nd_2Fe_{13}B_x$.
   b. a Nd-rich intergranular phase of composition $Nd_{24}FeB_x$.
   c. a phase within the matrix of composition $Nd_{12}Fe_5B_x$.

4. On ageing at 660°C the phase within the matrix disappeared.

5. Microhardness studies showed that two peaks occur for bulk material which has been aged at 600°C.

6. The powder particle size was smallest for the BMO material. The HD material had a larger particle size which decreased with increasing hydrogenation pressure.

7. The ${}_iH_c$ values of samples aged at 570°C to 660°C showed a broad peak with ageing time. There were also peaks in the microhardness values with ageing time for the samples aged at 570°C to 660°C.

8. The sample aged at 540°C showed a continuous fall in ${}_iH_c$ and microhardness with ageing time and might be associated with the fact that this temperature is below the melting point of the Nd-rich intergranular phase.

9. The samples aged at 570°C to 660°C exhibited three phases:
   a. a matrix phase of composition $Nd_2Fe_{12.4}B_x$. ($NdFe_{6.2}B_x$)
   b. a Nd-rich intergranular phase.
   c. a phase within the matrix which had a composition in the range $NdFe_4B_x$ to $NdFe_{2.2}B_x$.

10. The phase described in 9c disappeared on ageing at 660°C.

CHAPTER NINE

CONCLUSIONS

9.1 The $Sm_2(Co,Cu,Fe,Zr)_{17}$-type Alloy

9.1.1 The Microstructure of the $Sm_2(Co,Cu,Fe,Zr)_{17}$-type Alloy

The investigation has confirmed the nature of the microstructure in bulk and sintered samples of this alloy, namely that three phases exist each of which play an important role in the magnetic properties of the alloy. The three phase have been summarised in section 7.13 but it is worthwhile describing them again:

1. A Fe,Co-rich matrix phase.
2. A Sm, Cu-rich precipitate phase.
3. A Zr-rich platelet phase.

The extent of the porosity in the sintered samples was found to be dictated by two variables:

1. The initial powder size.
2. The temperature of sintering and solid solution treatment.

As expected, the initial powder size is the most important step in the processing procedure, as this dictates the final density values and therefore the BH_{max} values.

9.1.2 The Effects of Microstructure on the Magnetic Properties

Previous investigations on the "2:17"-type alloys have all concluded that the Sm, Cu-rich precipitate phase is associated with the pinning of domains which in turn is responsible for the coercivity values. However, this investigation has shown too that the presence of the Zr-rich phase plays an important role, as indicated by the deterioration in the magnetic properties, concurrent with the absence of this phase on ageing at 900°C.

9.1.3 The Effects of Heat Treatments on the Magnetic and Physical Properties

It was found that the S.S.T. temperature played a large role in terms of the magnetic properties, and it can be concluded that the development of the magnetic properties are dependent upon the condition of the microstructure after quenching from the S.S.T. temperature. The use of a pre-sintering temperature improved the remanence and maximum energy product values by increasing the densities of the sintered specimens.

The effects of ageing temperature on the magnetic and physical properties showed that at on ageing at 900°C, the variations of properties with ageing time were different due to the absence of the Zr rich phase. It can be concluded that the ageing temperature plays a major role in the growth and distribution of coherent precipitates during the ageing time interval as shown by the variations in $_iH_c$ and microhardness. The peaks in the variations of these properties with

ageing time are due to the pinning of domains and dislocations respectively.

There is also an effect on the electrical resistivity of the alloy on ageing and this appears to be related to the transformation of the precipitates from coherent to incoherent.

9.1.4 The Hydrogen Decrepitation Process

As mentioned in section 9.1.1, the initial particle size is of prime importance in these alloys, principally to achieve a high density and therefore high BH_{max} value (arising mainly from a high remanence value).

The hydrogen decrepitation process followed by ball milling produced particles of a larger size than BMO material, and consequently the HD samples had poorer magnetic properties. The size of the HD material will be strongly influenced by the initial grain size of the ingot material.

9.2 The Nd-Fe-B-type Alloy

9.2.1 The Microstructure of the Nd-Fe-B-type Alloy

The investigation showed that the two principal phases in this alloy were:

1. A matrix phase of approximate composition: $Nd_2Fe_{14}B$
2. An intergranular Nd-rich phase.

Another phase was observed within the grains and was found to be richer in Fe, this phase possibly corresponded to the phase observed by other workers (see for example, ref. 91).which is boron-rich with respect to the matrix.

As in the case of the "2:17"-type alloy, the porosity in the sintered samples was dependent on the initial powder particle size.

9.2.2 The Effects of Microstructure on the Magnetic Properties

It was found that the ageing temperature of 600°C produced the optimum magnetic properties. At an ageing temperature of 540°C no magnetic properties developed during the ageing time interval and it may be concluded that this is concurrent with a difference in microstructure at 540°C.

9.2.3 The Effects of Heat Treatments on the Magnetic and Physical Properties

It was found that the ageing temperature had a larger effect on the magnetic properties. During ageing above 570 °C the ${}_iH_c$ values developed a broad peak. The microhardness values also increased and decreased over a broad ageing time period. These variations however, were not in as good an agreement with the microhardness and ${}_iH_c$ correlations in the "2:17"-alloy. Thus, the coercivity mechanism is not as clearly defined in the Nd-Fe-B alloy system.

9.2.4 The Coercivity Mechanism in the Nd-Fe-B Alloy

The results of this investigation suggest a number of mechanisms occurring during ageing and these are outlined below.

1. On ageing at 570°C to 660°C, there occurs a two stage hardening process involving precipitation of two types of precipitate. This accounts for the "two-microhardness peak" phenomenon and the peak in coercivity on ageing.

2. On ageing, there is a solute redistribution, from the matrix phase, this however, does not explain the two microhardness peaks.

3. On ageing, there is some change in the surface morphology of the intergranular phase, so that reverse domain nucleation is more difficult, thus there is an increase in ${}_iH_c$ which may consequently decrease due to:

a. oxidation of the Nd-rich phase

b. a further change in the phase morphology.

4. There is a dual coercivity mechanism involving reverse domain nucleation and the pinning of domain walls.

There are a number of other possibilities, and it is evident that further work (particularly TEM) is required to study the microstructure after various ageing treatments.

9.2.5 The Use of Hydrogenation as a Means of Producing Permanent Magnets

As in the case of the "2:17"-type alloy discussed in section 9.1.4, a prime need of the HD process is to produce small particle sizes. In addition the highly reactive surfaces of the Nd-Fe-B alloy after HD means that certain processing steps could be used to make permanent magnets, namely:

1. HD at different pressures.

2. The handling of the powder after HD should be carried out in a vacuum or inert atmosphere to negate any contamination possibilities.

3. Control of the grain size of the bulk alloy during casting so that on hydrogenation smaller particle sizes could be achieved. For example, a small particle size would be obtainable from melt-spun material.

APPENDICES

APPENDIX A

APPENDIX A: Procedure for Pressurising a Sample in the High-Pressure Rig.

The procedure for pressurising a sample up to 2000 atms of H_2 pressure by the supply pressure of 100 atms is as follows:

1) A sample is introduced to a sample chamber S (see Fig. 6.5).

2) The chamber is flushed with hydrogen on several occasions to rid of air. (The pipe bore is 5.08×10^{-4} m and cannot be effectively evacuated).

3) 100 atms of hydrogen pressure are allowed past valve A and on to valve C. Valve I is initially open to allow the piston T to be driven back to its starting position at point 1, valves I and B are then closed.

4) The hydraulic pump W is operated which drives the piston T towards its finishing position at point 2. This action compresses the gas initially held in the piston chamber into a smaller volume, thus increasing the pressure. As long as the piston does not rest on the ends at position 1 or 2, the Budenberg hydraulic pressure gauge will register the pressure held within the system. A small magnetic rider R shows the position of the piston within the chamber.

5) Having completed a piston traverse from position 1 to position 2, valve F is closed and valves I and then B are opened and 100 atms is again opened to the system; driving the piston back to position 1.

6) Valve I and then valve B are shut and valve F opened and

the pressure further increased. The sample chamber need see no drop in pressure but only a gradual increase if valve F is kept closed until the Budenberg gauge shows the same or a higher pressure than previously shown at the end of the preceeding cycle.

7) The process is repeated until the required pressure is reached. Valve H may then be closed and valve I opened thus allowing the pump to be unpressurised while still registering the system's pressure via the Budenberg gauge.

8) To depressurise, valve H is opened. Once the piston is back at position 1, valve E is closed and valve C opened slowly, allowing the gas from the sample chamber to be vented to air.

All valves and piping are high pressure piping rated at 5000 atms. All hydrogen retaining piping, valves and sample chambers are of 316 stainless steel which exhibits a resistance to hydrogen embrittlement. Low pressure supply tubing is copper rated at 2000 atms.

The rate of rise of pressure is related to the ratio of sample chamber free volume to piston traverse volume. The smaller this ratio the faster the pressure rise. The sample chamber free volume is therefore kept to a minimum. This has two advantages; firstly the rate of rise of pressure is a maximum and secondly a small free volume of gas is safer in case of rupture.

APPENDIX B

APPENDIX B: Circuit for Double Channel Integrator.

The double channel integrator circuit consists of two separate channels each powered by its own 9 volt battery supply. The following key refers to both the field integrator and the B and B-H integrator, components of Fig. B1.

All IC's are TL081CP.

P_1 and P_3 are wire wound, 10 turn helipots and are incorporated for zero adjustment.

P_2 and P_4 are small carbon trimpots.

P_5 is a carbon potentiometer.

S_1 and S_2 are gain controls, x 1, x 10, x 100.

S_5 selects B or B-H mode of measurements.

S_3 and S_4 are integrator zeroing button switches normally off mode.

The power supply switches are double pole, double throw switches and are not shown in Fig. B1.

(i) Field Integrator.

A voltage is developed across L_o proportional to dH/dt and the integral of this voltage is proportional to ΔH, where H is the applied field.

I.C.1 integrates the input voltage and I.C.2 amplifies it and the resultant output voltage is proportional to ΔH.

With the coils out of the magnet pole pieces and the gain turned up to maximum, adjustment of the zero drift may be made. The power

should be turned on for approximately 10 minutes before zero adjustment is made.

(ii) B and B-H Integrator.

The circuitry is identical to that of the field integrator except that:-

S_5 switches between B and B-H mode, and P_5 adjusts the output of the field coil L_2 to equal the output of the B coil L_1, when a specimen is absent and the applied field is swept up.

The coil L_1 is the sample coil and has 2000 turns of 45 swg copper wire on a P.T.F.E. former of wall thickness 0.125 mm. The coil L_2 is empty and is identical to L_1.

L_1 and L_2 are connected in opposite senses and are adjusted using P_5 to give zero output when a sample is absent. The adjustment is generally done using more gain than necessary.

When a specimen is present the output is proportional to $4\pi M$ that is B-H.

L_3 is empty and has 2000 turns of 45 swg copper wire on an identical former to those of L_1 and L_2. The coil L_3 approximately compensates for the gap between the specimen and the coil of L_1. It is connected in the opposite sense to L_1 and the output is therefore proportional to B actually in the specimen.

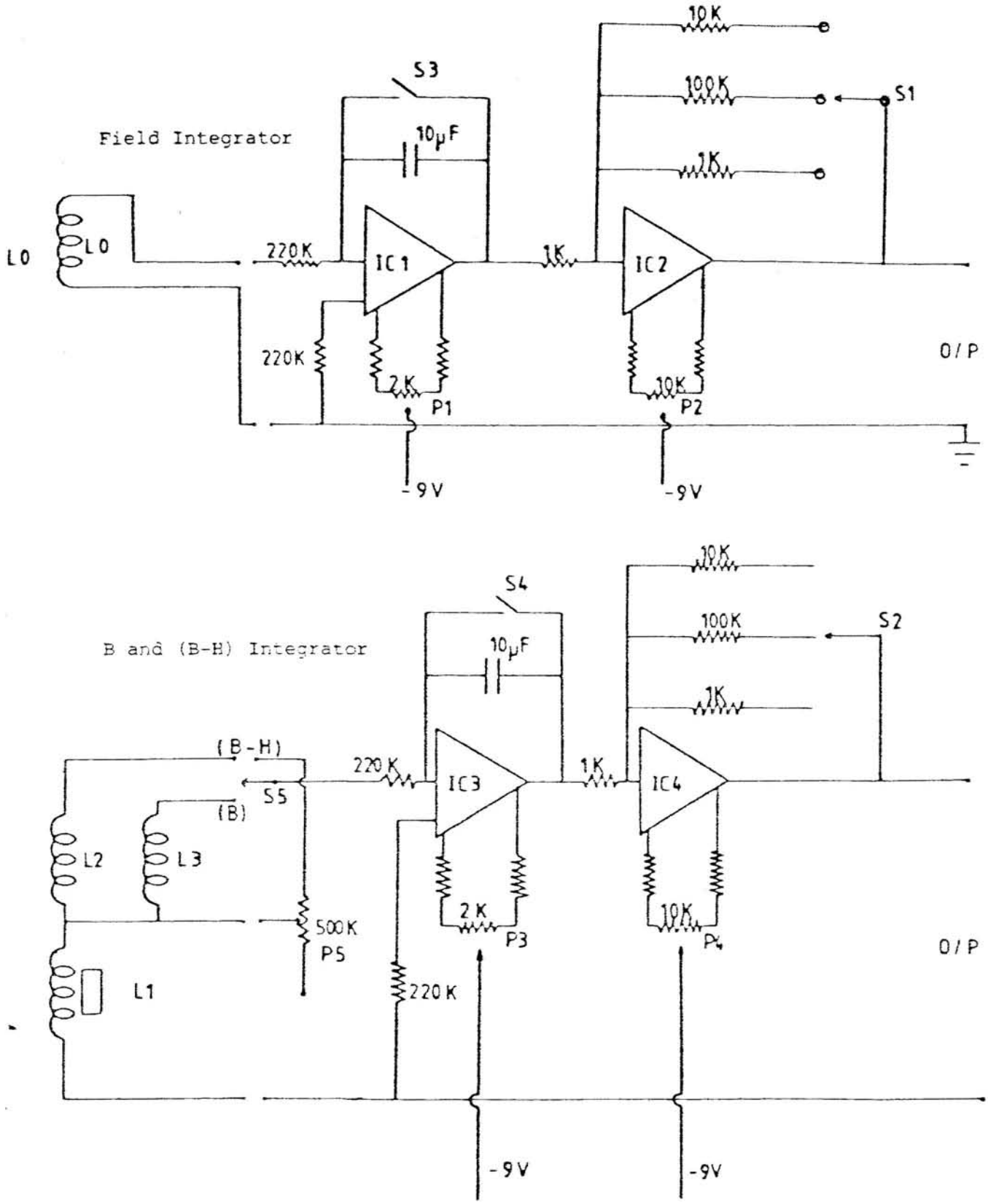

Fig. B1 Circuit diagram for double channel integrator.

TWO CHANNEL SELECTOR FOR

COMPUTER/OMNIBUS

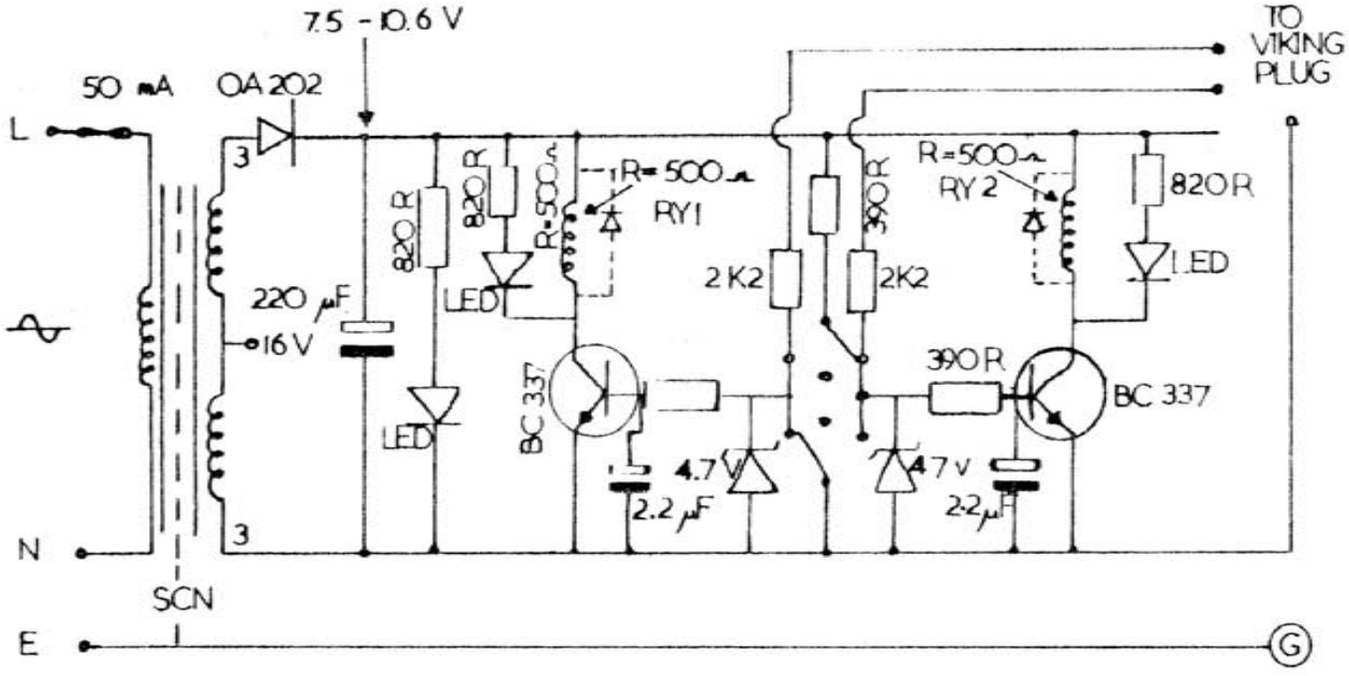

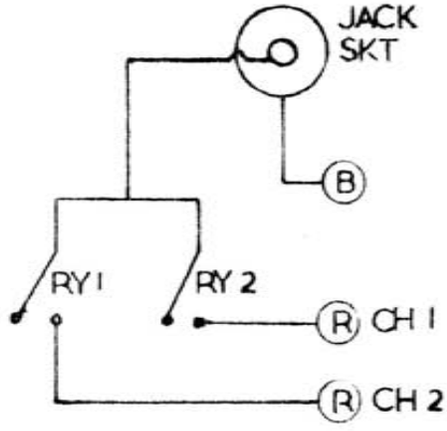

VIKING CONNECTIONS:

SCREEN	-	B28
RED CH1	-	B1
BLUE CH2	-	B3

Fig. B2

APPENDIX C

COMPUTER LISTING

```
3 PRINT:PRINT:PRINT
5 PRINT"        M A G N U M       "
7 PRINT:PRINT:PRINT
9 PRINT" INTERFACE PROGRAM :"
10 PRINT:PRINT
11 PRINT" WILL ACCEPT AND PROCESS DATA"
13 PRINT" FROM THE EQUIPMENT OPPOSITE;"
15 PRINT" ALSO LISTING AND PLOTTING THE"
17 PRINT" DATA ON THE ACCOMPANYING HARDWARE."
19 PRINT:PRINT:PRINT
50 DIM W1(200),U1(200),V1(200)
70 DIM W2(200),U2(200),V2(200),V3(200)
80 DIM U3(200),U4(200)
90 DIM E(200),F(200),G(200),U(200),V(200)
100 DIM A$(200),B$(200),U$(200)
150 DIM AS(200),BV(200)
250 PRINT
260 INPUT"TYPE IN SAMPLE DESCRIPTION";U$
270 PRINT
300 SS=1500
350 PRINT
400 DF=1
450 PRINT
455 C1=14.03
456 C2=37.253
475 PRINT
500 PRINT"TYPE IN SAMPLE LENGTH & DIAMETER IN CMS"
505 INPUT LE,DI
510 LF=0.413/(((DI/2)↑2)*3.142*LE)
550 PRINT
600 N$="1"
700 M$="2"
750 OPEN 1,8
800 FOR  C=1TO 100
1000 PRINT#1,M$
1100 FOR I=1TO SS
1200 NEXT I
1300 INPUT#1,A$(C)
1400 FOR I=1 TO SS
1500 NEXT I
1600 PRINT#1,N$
1700 FOR I=1 TO 500
1800 NEXT I
1900 INPUT#1,B$(C)
1910 W1(C)=(VAL(A$(C))/1000)
1915 U1(C)=-C1*(W1(C))
1920 V1(C)=(INT(100*(U1(C)-.005)))/100
1925 W2(C)=(VAL(B$(C))/1000)
1930 U2(C)=(C2*(W2(C)))*DF*LF
1935 V2(C)=(INT(100*(U2(C)+.005)))/100
1940 U3(C)=(U1(C)+U2(C))*(U1(C))
1945 V3(C)=(INT(100*(U3(C)-0.005)))/100
1950 U4(C)=U3(C)/U1(C)
2000 IF VAL(B$(C))<=000 THEN GOTO 2100
```

```
2010 FOR I=1 TO SS
2020 NEXT I
2050 NEXT C
2100 PRINT"WHICH VARIABLE IE B,M OR B-H VS H ?"
2102 CLOSE 1,8
2200 INPUT T$
2250 INPUT"DO YOU REQ A SCREEN DATA LIST";M$
2270 IF M$="Y" THEN GOTO 2300
2280 INPUT"DO YOU REQ THE MAG PARAMS";S$
2285 IF S$="Y" THEN GOTO 2500
2290 GOTO 3050
2300 PRINT:PRINT"DATA  ";U$
2350 PRINT:PRINT
2400 PRINT" H  (KOE)   ";T$;"(KG)"
2450 PRINT:PRINT
2500 FOR F=1TO C
2770 IF S$="Y" THEN GOTO 2900
2800 PRINTV1(F);"     ";V2(F)
2900 NEXT F
2902 CBH=0
2904 FOR F=1TO C
2914 IF CBH>.5THEN GOTO 2970
2918 IF F<1.5 THEN GOTO 2952
2919 B1=U3(F)-U3(F-1)
2920 IF B1<0 THEN GOTO 2952
2922 PRINT
2924 B2=V3(F-1)
2926 PRINT"BH MAX=";-B2;"(MGOE)"
2928 CBH =CBH+2
2934 PRINT
2952 NEXT F
2970 RE=(INT(100*(V2(1)+(V1(1)*((V2(1)-V2(2))/(V1(2)-V1(1)))))))*0.01
2971 PRINT"REMANENCE=";RE;"(KG)"
2972 SQ=(INT(100*(-B2/RE↑2+.005)))*0.01
2973 PRINT
2974 PRINT"SQ.RATIO(BHMAX/REM↑2)=";SQ
2975 GOSUB 30400
2977 PRINT
2980 PRINT"INTRINSIC COERCIVITY=";-CO
2985 PRINT
2990 GOSUB 30200
3000 PRINT"SQ.FACTOR(H FOR 90% REM/INT COERC)=";PS
3010 PRINT
3015 GOSUB 30600
3020 PRINT"INDUCTION COERCIVITY=";RC;"(KOE)"
3025 PRINT
3050 INPUT"DO YOU REQ A SCREEN GRAPH PLOT";C$
3100 IF C$="Y" THEN GOTO 3400
3200 INPUT"DO YOU REQ MORE DATA";C$
3300 IF C$="Y" THEN GOTO 250
3350 GOTO 12000
3400 INPUT"TYPE IN MAX X,Y AXES VALUES";Y,X
3500 FOR F=1TO C
3600 E(F)=INT((V1(F)/Y)*28)
3700 F(F)=INT((V2(F)/X)*20)
3800 G(F)=INT(34703-E(F)-(40*F(F)))
3900 NEXT F
```

```
4000 FOR N=1 TO 15
4100 PRINT:PRINT
4200 NEXT N
4300 T=34703
4350 POKE 34729,8
4400 I=34676
4500 POKE I-1,107
4600 FOR K=1TO 4
4700 FOR X=I TO I+5
4800 POKE X,64
4900 NEXT X
5000 I=I+6
5100 POKE I,91
5200 I=I+1
5300 FOR Y=T TO T-160 STEP-40
5400 POKE Y,93
5500 NEXT Y
5600 T=T-199
5700 POKE T,70
5800 T=T-1
5900 NEXT K
6000 POKE T,70
6100 FOR F=1 TO C
6200 POKE G(F),86
6300 NEXT F
6400 PRINT:
12000 INPUT"DO YOU REQ A GRAPH PRINTOUT";D$
12200 IF D$="Y" THEN GOTO 12600
12300 INPUT"DO YOU REQ MORE DATA";C$
12400 IF C$="Y" THEN GOTO 250
12500 GOTO 16000
12600 INPUT"DO YOU REQ AXES DRAWN";L$
12610 IF L$="N" THEN GOTO 15220
12612 INPUT"MAX:15 OR 5";Q$
12620 SYS 9*4096
12700 P=143:Q=200
12710 Q=Q+18
12720 !MA,P,Q
12725 !PR,"B-H (KG)"
12730 P=160:Q=200
12800 !MA,P,Q
12810 IF Q$="5" THEN GOTO 12815
12812 GOTO 12900
12815 !PR,"L 5"
12817 GOTO 13100
12900 !PR,"L 15"
13100 !MA,P,Q
13200 FOR I=1TO5
13300 Q=Q-32
13400 !DA,P,Q
13450 IF I=5THEN GOTO 13600
13500 !PR,"-"
13600 !MA,P,Q
13700 NEXT I
```

```
13800 Q=Q-2
13810 P=P-2
13815 !MA,P,Q
13820 !PR,"T"
13900 Q=Q+5
13950 !MA,P,Q
14000 FOR I=1 TO 5
14100 P=P-31
14200 !DA,P,Q
14300 Q=Q-5
14400 !MA,P,Q
14500 !PR,"T"
14600 Q=Q+5
14700 !MA,P,Q
14750 NEXT I
14800 R=1:S=30
14850 !MA,R,S
14854 IF Q$="5"THEN GOTO 14860
14856 GOTO 14900
14860 !PR,"5"
14865 GOTO 14950
14900 !PR,"15"
14950 R=R+70
15000 !MA,R,S
15050 !PR,"- H (KOE)"
15100 R=R+92
15120 S=S+6
15150 !MA,R,S
15200 !PR,"0"
15210 IF L$="Y" THEN GOTO 15250
15220 INPUT"MAX:15 OR 5";Q$
15225 SYS 9*4096
15250 FOR F=1 TO C
15266 U(F)=INT(160-(U1(F)/(-VAL(Q$)))*153)
15269 V(F)=INT(160*(U2(F)/(VAL(Q$)))+43)
15400 P=U(F)
15450 Q=V(F)
15500 IF F<1.5 THEN GOTO 15552
15550 GOTO 15700
15552 W=INT(160*(RE/(VAL(Q$)))+43)
15600 Z=160:N=W
15605 !MA,Z,N
15610 !DA,P,Q
15650 NEXT F
15660 GOTO 15800
15700 IF F=C THEN GOTO 15710
15705 GOTO 15740
15710 Q=43
15740 !DA,P,Q
15750 NEXT F
15800 !HO
15850 !KI
16000 INPUT"DO YOU REQ A B VS H PLOT";C$
16002 IFC$="Y"THEN GOTO 16006
16004 GOTO 16090
16006 SYS9*4096
```

```
16010 Z=160:N=W
16012 !MA,Z,N
16013 FOR F=1TOC
16014 BV(F)=INT(160*U4(F)/VAL(Q$)+43)
16016 BP=U(F)
16018 BQ=BV(F)
16020 IF U4(F)<=0THEN GOTO 16028
16022 !DA,BP,BQ
16023 NEXT F
16028 BQ=43
16029 BP=INT(160+(RC/(-VAL(Q$)))*153)
16030 !DA,BP,BQ
16032 !HO
16034 !KI
16090 INPUT"DO YOU REQ A DATA PRINTOUT";Y$
16100 IF Y$="Y" THEN GOTO 16300
16150 INPUT"DO YOU REQ THE MAG PARAMS PRINTED";K$
16175 IF K$="Y" THEN GOTO 16720
16200 GOTO 30000
16300 OPEN 3,4
16305 PRINT#3,
16308 PRINT#3,
16310 PRINT#3,U$
16315 PRINT#3,
16350 PRINT#3,"        ";"-H";"(KOE)                ";T$;"(KG)"
16370 PRINT#3,
16400 FOR F=1 TO C
16600 PRINT#3,"        ";-V1(F);"                ";V2(F)
16700 NEXT F
16705 PRINT#3,
16710 CLOSE 3,4
16720 OPEN 3,4
16725 IF Y$="N" THEN GOTO 16730
16728 GOTO 16800
16730 PRINT#3,U$
16735 PRINT#3,
16800 PRINT#3,"    REMANENCE=";RE;"(KG)"
16850 PRINT#3,
16900 GOSUB 30400
17000 PRINT#3,"    INTRINSIC COERCIVITY=";-CO;"(KOE)"
17005 PRINT#3,
17010 GOSUB 30600
17020 PRINT#3,"    INDUCTION COERCIVITY=";RC;"(KOE)"
17050 PRINT#3,
17310 GOSUB30200
17320 PRINT#3,"    SQ.FACTOR(H90%REM/INT.CO)=";PS
17400 CBH=0
17500 FOR F=1TO C
17600 IF CBH>0.5THEN GOTO 30000
17700 IF F<1.5 THEN GOTO 18400
17800 B1=V3(F)-V3(F-1)
17900 IF B1<0 THEN GOTO 18400
18000 PRINT#3,
18100 B2=V3(F-1)
18200 PRINT#3,"    BH MAX=";-B2;"(MOOE)"
```

```
18250 CBH=CBH+2
18290 PRINT#3,
18300 PRINT#3,"    SQUARENESS RATIO (BHMAX/(REM*REM))=";SQ
18400 NEXT F
30000 CLOSE 3
30050 INPUT "DO YOU REQ THE INFO AGAIN";K$
30100 IF K$="Y" THEN GOTO 2250
30150 END
30200 SE=RE*0.9
30210 FOR F=1TO C
30220 AS(F)=SE-V2(F)
30230 IF AS(F)>=0THEN GOTO 30250
30240 NEXT F
30250 GR=(V2(F)-V2(F-1))/(V1(F)-V1(F-1))
30260 HK=V1(F-1)-((V2(F-1)-SE)/GR)
30265 GOSUB30400
30270 PS=(INT(100*(HK/CO+.005)))*.01
30280 RETURN
30400 CO=V1(C)-(V2(C)*((V1(C)-V1(C-1))/(V2(C)-V2(C-1))))
30450 CO=(INT(100*(CO-.005)))/100
30500 RETURN
30600 FORF=1TOC
30700 IF U4(F)<=0 THEN GOTO 30900
30800 NEXT F
30900 RC=V1(F)
31000 RG=(U4(F-1)-U4(F))/(V1(F-1)-V1(F))
31100 RC=V1(F)-(U4(F)/RG)
31200 RC=-(INT(100*(RC-0.005)))/100
31300 RETURN
35000 END
READY.
```

APPENDIX D

APPENDIX D: Calibration of magnet current versus magnetic field

Magnet current (A) ± 0.05	Magnet field ±0.05 (KOe)	A$ Omnibus OB2 ±0.002 digital value
0	0.18	0.011
0.1	1.75	0.077
0.2	3.30	0.155
0.3	5.05	0.239
0.4	6.8	0.318
0.5	8.3	0.3945
0.6	9.5	0.469
0.7	10.5	0.539
0.8	11.5	0.600
0.9	12.0	0.655
1.0	12.5	0.700
1.1	13.0	0.731
1.2	13.5	0.762
1.3	13.7	0.788
1.4	14.0	0.809
1.5	14.3	0.830

Average gradient for magnetfield/digital reading = 16.005.

Therefore conversion for digital reading to a field reading is

$H = -16.005A\$$ A$ is the read in value of magnetic field in mV equivalent

Using a pure Ni standard:

At saturation: $4\pi M_s = 6.185$ KG/$_{cc}$; corresponding average digital reading B$, equals 0.149, this is for 0.413cc of pure Ni; therefore 1cc of material.

$B-H = 4\pi M = \frac{6.184}{0.149} B\$ = 41.503 B\$.$ B$ is the read in value of magnetic intensity in mV equivalent

REFERENCES

1. O. Christensen, Final Report of Erhrervsforskernddannelse, 18-75, (1978) pub. no. 7805.
2. Y. Iwama, Proc. of 5th Intl. Workshop on RE-Co PM and applic. (1981) pp. 283.
3. K.J. Strnat, Proc.4th Intl. Workshop on RE-Co-PM and applic. (1979) pp.8.
4. H. Sasaki, Y. Kinonchi, Proc. 4th Intl. Conf. on RE-Co-PM and applic. (1979) p.83.
5. H. Winkler, Proc. of CEC Workshop on Nd-Fe PMs, Brussels (1984) pp. 25.
6. J.M.D. Coey, Proc. of CEC Workshop on Nd-Fe-B PMs, Brussels (1984) pp. XI.
7. B.D. Cullity, "Introduction to Magnetic Materials", Addision-Wesley.
8. M. McCaig, "Permanent Magnets in Theory and Practice", Pentech Press.
9. L.F. Bates, "Modern Magnetism", Cambridge University Press.
10. J.D. Livingston, J. App. Phys. 52 (1981) pp. 2544.
11. J.J. Becker, J. App. Phys..39 (1968) pp. 1270.
12. H. Zijlstra, J. App. Phys. 41 (1970) pp. 4881.
13. J.D. Livingston, AIP Conf. Proc. 10(1) (1972) pp. 643.
14. C. Kittel and J.K. Galt, Sol. Stal. Phys. 3 (1956) pp. 437.
15. S. Shtrikman and D. Treves, J. App. Phys. 31 pp. 72S (1960).
16. J.J. Becker, IEEE Trans. MAG 5 (1969) pp. 211.
17. D.I. Paul, J. App. Phys. 53(3) (1982) pp. 2362.
18. J.J. Becker, J. App. Phys. 41(3) (1970) pp. 1055.
19. R. Lemaire et al., J. App. Phys. 39(7) (1968) pp. 1092.
20. Y. Khan, Acta. Cryst. B29 (1973) pp. 2502.
21. K. Nassau L.V. Cherry et al., J. Phys. Chem. Sol. 16 (1960) pp. 123.

22. K.H.J. Buschow and A.S. Van der Goot, J. Less. Comm. Met. 14 (1968) pp. 323.

23. T. Nishio et al., Proc. 4th Intl. Workshop on RE-Co PM and applic. (1979) pp. 271.

24. D.T. Cromer and A. Larson, Acta Cryst. 12 (1959) pp. 855.

25. K.H.J. Buschow and F.J.A. den Broeder, J. Less Comm. Met. 33 (1973) pp. 191.

26. K. Kuhn and A.J. Perry, Metal Science, 9 (1975) pp. 339.

27. K.H.J. Buschow, J. Less Comm. Met. 25 (1971) pp. 131.

28. A.J. Perry, J. Less Comm. Met. 51 (1977) pp. 153.

29. H. Nagel, A.J. Perry and A. Menth, J. App. Phys. 47 (6) (1976), pp. 2662.

30. E.A. Nesbitt, J. App. Phys. 40 (1969) pp. 1259.

31. J.D. Livingston and D.L. Martin, J. App. Phs. 48(3) (1977) pp. 1350.

32. J.H. Wernick and S. Geller, Acta Cryst. 12 (1959) pp. 662.

33. K.A. Gschneider and R.M. Valleta, Acta Met. 16 (1968) pp. 477.

34. K.H.J. Buschow and A.S. van der Goot, J. Less Comm. Met. 17 (1969) pp. 249.

35. K.J. Strnat, Cobalt 36 (1967) pp. 119.

36. K.H.J. Buschow, J. Less Comm. Met. 11 (1966) pp. 204.

37. E.F. Bertrant, R. Lemaire and J. Schweizer, Bull. Soc. Fr. Miner. Cryst. 68 (1965) pp. 580.

38. K.H.J. Buschow and W.A.J.J. Velge, J. Less Comm. Met. 13 (1967) pp.11.

39. K.H.J. Buschow, Philips Res. Rep. 26 (1971) pp. 49.

40. R.W. Lee, J. App. Phys. 52 (1981) pp. 2549.

41. D. Givord, Proc. of CEC Workshop on Nd-Fe PM: Future and Applications, Brussels (1984) pp. 131.

42. G. Hoffer and K.J. Strnat, IEEE Trans. MAG2 (1966) pp. 487.

43. K.J. Strnat, Cobalt 36 (1967) pp. 133.

44. K.J. Strnat, Proc. 2nd Intl. Workshop on RE-Co Pm and Applic. (1976) pp. 5.

45. D. Das, IEEE Trans. MAG5 (1969) pp. 214.

46. C.M. McFarland, Proc. 10th RE research conf (1973) VII pp. 692.

47. R.E. Cech, J. Met. 26 (1974) pp. 32.

48. Y. Tawara, H. Senno, Proc. 2nd Intl. Workshop on RE-Co PM and applic. (1976) paper no. V-1.

49. K. Bachmann and H. Nagel, Proc. 2nd Intl. Workshop on RE-Co PM and applic. (1976) paper No. IV-2.

50. T. Yoneyma, S. Tomizawa et al., Proc. 3rd Intl. Workshop on RE-Co PM and applic. (1978) pp. 406.

51. G.C. Hadjipanayis et al. Proc. 6th Int. Workshop on RE-Co PM and applic. (1982) pp. 667.

52. A.E. Ray, J. App. Phys, 55(6) (1984) pp. 2094.

53. T. Yoneyma et al., Proc. 4th Intl. Conf. on RE-Co PM and applic. (1979) pp. 407.

54. K.J. Strnat and A.E. Ray, Goldschmidt Informiert 4/75 (1975) pp. 47.

55. H. Senno and Y. Tawara, IEEE Trans. MAG-10 (2) (1974) pp. 313.

56. E. Potenziani et al., IEEE Trans. MAG 18 (6) (1982) pp. 1457.

57. J.D. Livingston, IEEE Trans. MAG 14 (1978) pp. 668.

58. H. Nagel and A. Menth, IEEE Trans. Mag 14 (1978) pp. 671.

59. K.N. Melton and H. Nagel, J. App. Phys. 48 (1977) pp. 2608.

60. H. Krönmüller et al., IEEE Trans. Mag. MAG 20 (1984) pp. 1569.

61. I.T. Oiwa et al., Proc. 11th RE research conf. Traverse City (1974) pp. 353.

62. T. Ojima et al., IEEE Trans. MAG 13 (1977) p. 1317.

63. M.V. Satyanarayana et al., J. App. Phys. 53(3) (1982) pp. 2374.

64. G.C. Hadjipanayis, J. App. Phys. 55(6) (1984) pp. 2091.

65. T. Yoneyma et al., Ferrites: Proc. of Intl. Conf. Sept-Oct. (1980) pp. 362.

66. T. Bailey and I.R. Harris, to be published.

67. A. Kianvash and I.R. Harris, J. Mat. Sci. Lett. 3 (1984) pp. 18.

68. R.K. Mishra and G. Thomas, Proc. 4th Intl. Workshop on RE-Co PM and applic. (1979) pp. 301.

69. L. Rabenburg, R.K. Mishra and G. Thomas, J. App. Phys. 53(3) (1982) pp. 2389.

70. A. Kianvash and I.R. Harris, J. Less. Comm. Met. 98 (1984) pp. 93.

71. G.C. Hadjipanayis et al., Proc. 6th Intl. Workshop on RE-Co PM and applic. (1982) pp. 609.

72. D. Li and K.J. Strnat, J. App. Phys. 55(6) (1984) pp. 2103.

73. T. Shimoda et al., Proc. 4th Intl. Conf. on RE-Co PM and applic. (1979) pp. 335.

74. Xiao Sen-tao et al., J. App. Phys. 52(3) 1981 pp. 2529.

75. Sun tian-duo, Proc. 6th Intl. Conf. on RE-Co PM and applic. (1982) pp. 433.

76. J.D. Livingston, J. App. Phys. 46(12) (1975) pp. 5259.

77. Sun Daku, and Liu Yujin, Proc. 5th Intl. Conf. on RE-Co PM and applic. (1981) pp. 525.

78. F. Rothwarf et al., Proc. 6th Intl. Conf. on RE-Co PM and applic. (1982) pp. 567.

79. A.L. Robinson, Science 223 (1984) pp. 920.

80. V.I. Chechernikov, N.M. Speronskiy, E.V. Maslova and V.F. Terekhova, Fiz. Metal. Metalloved. 20(2) (1965) pp. 299.

81. J.J. Croat, App. Phys. Lett. 39(4) (1981) pp. 357.

82. L. Potocky, L. Novak et al., J. Magn. Magn. Mat. 26 (1982) pp. 112.

83. N.F. Chaban, Yu. B. Kuzma et al., Dopov. Akad. Nauk. SSSR Ser. A. Fiz-Mat. Tekh. Nauki No. 10 (1979) pp. 873.

84. H.H. Stadelmaier, N.A. Elmasry and S. Cheng, Mat. Lett. 2(2) (1983) pp. 169.

85. G.C. Hadjipanayis, R.C. Hazelton, K.R. Lawless, J. App. Phys. 55(6) (1984) pp. 2073.

86. M. Sagawa et al., J. App. Phys. 55(6) (1984) pp. 2083.

87. J.F. Herbst, J.J. Croat, F.E. Pinkerton, Phys. Rev. B. 29(7) (1984) pp. 4176.

88. C. Noble and I.R. Harris, "Preliminary report on the constitution and hydrogen decrepitation properties of a Nd-Fe-B alloy". Dept. Metallurgy and Materials, University of Birmingham (1984).

89. I.R. Harris and T. Bailey, Proc. of CEC Workshop on Nd-Fe PMs Brussels (1984) pp. 99.

90. H.H. Stadelmaier, N.A. Elmasry, N.C. Liu and S.F. Cheng, Mat. Lett. 2(5A) (1984) pp. 411.

91. J. Ormerod, Proc. of CEC Workshop on Nd-Fe PMs Brussels (1984) pp. 69.

92. T. Bailey and I.R. Harris, J. Mat. Sci. Lett. 4 (1985) pp. 151.

93. D.J. Sellmyer, A. Ahmed, G. Muench and G. Hadjipanayis, J. App. Phys. 55(6) (1984) pp. 2088.

94. J.J. Croat, J.F. Herbst, R.W. Lee and F.E. Pinkerton, J. App. Phys. 55(6) (1984) pp. 2078.

95. J.J. Croat, J.F. Herbst, R.W. Lee and F.E. Pinkerton, App. Phys. Lett. 44(1) (1984) pp. 148.

96. A. Kianvash and I.R. Harris, J. Mat. Sci. 19 (1984) pp. 353.

97. T. Bailey and I.R. Harris, J. Mat. Sci. Lett. 4 (1985) pp. 645.

98. I.R. Harris, C. Noble and T. Bailey, J. Less Comm. Met. 106 (1985) L1-L4.

99. M. Sagawa et al., Proc. Intermag Conf. (1984) Hamburg.

100. A. Kianvash, Ph.D. Thesis, University of Birmingham (1983).

101. J.H. Zhu, T.D. Sun et al., Intermag Conf. (1984) Hamburg.

102. C. King, Ph.D. Thesis, University of Birmingham (1981).

103. A. Kianvash and I.R. Harris, J. Mat. Sci. 20 (1985) pp. 682.

104. A.E. Ray, Proc. 7th Intl. Workshop on RE-Co PMs and applic. (1983) pp. 261.

105. L. Rabenburg, R.K. Mishra and G. Thomas, Proc. 6th Intl. Workshop on RE-Co PMs and applic. (1982) pp. 559.

106. R. Lowe, M.Sc. Thesis, University of Birmingham (1982).

107. R.E. Smallman, "Modern Physical Metallurgy" (Butterworths 1980).

108. Z. Fisk, G.W. Webb, Treatise on Mat. Sci. and Tech. 21 Electronic Structure and Properties (ed. by F.Y. Fradin).

109. Metals Handbook Vol. 1 American Soc. Metals 8th ed. p. 817.

110. Sun Tian Duo, J. App. Phys. 52 (1981) pp. 2532.

111. Xu Wendi et al., Proc. 7th Intl. Conf. on RE-Co PMs and applic. (1983) pp. 347.

112. Chou Sochen Wang Run and Sun Guanfei, Proc. 6th Intl. Workshop on RE-Co PMs and applic. (1982) pp. 693.

113. R.E. Reed-Hill, "Physical Metallurgy Principles" (Van Nostrand, 1970).

114. H.W. King and S.G. Glover, J. Iron and Steel Inst. 196 (1960) pp. 281.

115. J. Burke, "The Kinetics of Phase Transformations in Metals", Pergamon Press Ltd. (1965).

116. M. Velicescu, Proc. 6th Intl. Conf. on RE-Co PMs and applic. (1982) pp. 341.

117. J. Hopkins, "A microstructural analysis of the NdFeB alloy 'Neomax'", Final Year Project Report, University of Birmingham, (1985).

118. M. Sagawa et al., Proc. 8th Intl. Conf. on RE magnets and applic. (1985) pp. 587.

119. A.J.W. Ogilvy, G.P. Gregon and H.A. Davies, Proc. of CEC Workshop on Nd-Fe PMs, Brussels (1984) pp. 93.

120. R.W. Lee, App. Phys. Lett. 46(8) (1985) pp. 790.

121. G.C. Hadjipanayis and Y.F. Tao, Proc. 8th Intl. Conf. on RE magnets and applic. (1985) pp. 657.

122. R.K. Mishra et al., Proc. (1985) Intermag. Conf. pp. AA-3.

123. K.D. Durst, H. Kronmüller, Proc. 8th Intl. Workshop on RE-magnets and applic. (1985) pp. 725.

124. D. Fruchart et al., Proc. CEC Workshop on Nd-Fe PMs, Brussels (1984) pp. 173.

125. J.D. Livingston, Proc. 8th Intl. Workshop on RE-magnets and applic. (1985) pp. 423.

126. J. Fidler, Proc. (1985) Intermag Conf. pp. AA-5.